1982

Simplified methods for the inelastic analysis and reliability assessment of stiffened shells

Fouad Shanouda Fanous
Iowa State University

Fanous, Fouad Shanouda

SIMPLIFIED METHODS FOR THE INELASTIC ANALYSIS AND RELIABILITY ASSESSMENT OF STIFFENED SHELLS

Iowa State University PH.D. 1982

Simplified methods for the inelastic analysis and reliability assessment of stiffened shells

by

Fouad Shanouda Fanous

A Dissertation Submitted to the
Graduate Faculty in Partial Fulfillment of the
Requirements for the Degree of
DOCTOR OF PHILOSOPHY

Department: Civil Engineering
Major: Structural Engineering

Approved:

Signature was redacted for privacy.

In Charge of Major Work

Signature was redacted for privacy.

For the Major Department

Signature was redacted for privacy.

For the Graduate College

Iowa State University
Ames, Iowa

1982

TABLE OF CONTENTS

INTRODUCTION

The purpose of the containment vessel in a nuclear power plant is to prevent the release to the atmosphere of any radioactivity which may accidentally be present within the vessel. The probability that the containment will not leak radioactivity must be acceptably low. The overall objective of this research, of which this dissertation forms a part, is to assess the uncertainty of the containment vessel resistance for nuclear power plants. The specific objective of the study presented herein is to develop simplified methods to describe the statistical characteristics of the resistance of steel containment vessels to internal static uniform and internal high intensity localized loading. This dissertation is composed of three papers, two of which have been published and the third which will be submitted for publication.

Part I. " Simplified Techniques for the Inelastic Analysis of Stiffened Shells Under Uniform Static Internal Pressure." The author intends to submit this paper to the Journal of Pressure Vessel Technology, American Society of Mechanical Engineers. This paper is devoted to developing simplified methods for predicting the resistance of stiffened axisymmetric shells under uniform internal static pressure. The development of these methods is based upon limit analysis theory and takes into account the effect of the large deformations. Finite element analysis is used to guide and calibrate these methods.

Part II. "Simplified Dynamic Analysis for Internal Locally Loaded Shells" was presented and published in the Proceedings of the International Workshop on Containment Integrity, which was held in Washington, D.C., USA, in June 1982. This paper concentrates on the dynamic analysis of unstiffened axisymmetric structures subjected to internal localized dynamic loads. Simplified methods for the prediction of the maximum strain ductility of cylindrical and spherical shells as well as circular plates under high intensity localized pulse are proposed. The methods are developed by idealizing the structure as an elastic-perfectly plastic single degree of freedom model and taking into consideration the effects of large deformations. Finite element analysis is used to guide and calibrate the proposed methods.

Part III. "Reliability Assessment of Containment Resistance" was presented and published in the Proceedings of the Pressure Vessel and Piping Conference sessions on pressure safety and reliability, American Society of Mechanical Engineering, which was held in Orlando, Florida, USA, in July 1982. This paper summarizes some reliability techniques and demonstrates their use to assess the uncertainty of the containment vessel resistance. A Monte Carlo simulation technique, an advanced second moment method and a simplified approach for practical analyses are proposed and compared.

In general, each paper provides several numerical examples which explain and demonstrate the use of the proposed simplified methods. Additionally, each paper includes a bibliography related to the specific

topic. Also, the supplementary appendices for the papers provide more details regarding some specific problems. For example, the Part I appendix gives the details for the prediction of the limit pressure for internally loaded stiffened conical shells. Also, the appendix of Part II summarizes studies conducted to investigate the effect of the finite element mesh as well as the time step size on the nonlinear transient dynamic analysis results.

PART I. SIMPLIFIED TECHNIQUES FOR THE INELASTIC ANALYSIS OF STIFFENED SHELLS UNDER UNIFORM STATIC INTERNAL PRESSURE

Abstract

Simplified methods for predicting the resistance of stiffened axisymmetric shells are presented. A uniform internal static pressure is considered and strain ductility is taken as the failure criteria. The development of these methods is based upon limit analysis theory and takes into account the effects of large deformations. Twelve axisymmetric models are analyzed using the finite element technique and the results are used in the calibration of the simplified solution. An analysis of a typical pressure vessel is performed by the proposed and the finite element methods. The results of the pressure vessel analysis, as well as those for the twelve models, illustrate the agreement between the finite element and the simplified methods.

Introduction

The problem of evaluating the resistance of stiffened axisymmetric shells under uniform internal pressure is an important one, particularly with regard to steel containment vessels for nuclear power plants. The solution could require a three-dimensional finite element analysis which takes into account material and geometric nonlinear effects. While this is theoretically possible, it would be expensive in terms of computer time; therefore, another alternative is useful. Additionally, finite element models are difficult to incorporate into reliability predictions. An alternative approach is to use basic shell theory in conjunction with the limit analysis techniques to solve for the result-

ing shell resistance. Several analytical studies have dealt with various methods of computing the resistance of stiffened axisymmetric shells. Most of these studies have evaluated the limit pressure for such types of structures using the Tresca yield criteria and ignoring the effect of geometric deformations. Paul and Hodge (1) found an expression for the limit pressure of a uniformly loaded cylinder with simply supported ends. The problem of a cylindrical shell built-in at one end, free at the other and subjected to uniform pressure along with an independent axial load was studied by Oant (2) and Hodge and Panarelli (3). A solution of an axisymmetric shell jointed at both ends to a rigid plate is given in (4). Cylindrical shells without axial load and with purely longitudinal ribs were treated by Biron and Sawczuk (5). A summary of the results obtained by these investigators and others are presented in Ref. (6). In this study, a method which is based upon the von Mises yield hypothesis and which considers material and geometric nonlinear effects is proposed.

The following study represents a portion of a total program, the objective of which is to assess the uncertainty of steel containment vessel resistance. Typically these containments are stiffened axisymmetric steel shells. To attain this goal, simplified analytical solutions based upon the formation of a limit mechanism were established. The development and calibration of these methods for stiffened cylindrical shells is given in detail. Equations for the prediction of the resistance of stiffened conical, ellipsoidal, spherical and torispherical shells are also given. Furthermore, a summary of the analysis of

a typical containment by the finite element method and the simplified approach is presented. In the total program, these simplified methods have been incorporated into a reliability assessment.

Containment Resistance

Failure of a containment is considered to occur when leakage of the containment occurs. Leakage will occur when a crack passes through the entire plate thickness of the containment vessel walls. The approach adopted by many investigators (7,8) is to assume that failure (leakage) will take place in the shell when deformation (displacement and/or strains) become large.

The question of whether to use displacement or strain as a basis for defining failure is certainly debatable (7). The ASME Code has provisions that allow the use of either or both (9,10). Highly localized bending strains have little effect on the collapse strength and may not be indicative of structure failure (8). On the other hand, strains are certainly more indicative of material distress than displacement. In this work strain, more particularly, the maximum circumferential membrane strain in the axisymmetric containment vessel, is selected as basis of failure indication.

To prevent the occurrence of large deformation or leakage in such vessels, it is necessary to restrict the magnitude of the maximum strain. The pressure at which the maximum allowable strain is reached is termed herein the containment vessel resistance or the plastic collapse pressure. Reference 7 recommends a value of two as the lower

limit of the strain ductility capacity (strain ductility = maximum strain/yield strain). The corresponding pressure is designated as $p_{2\varepsilon y}$. (See Fig. 1.)

Simplified Static Analysis of Stiffened Axisymmetric Shells

General

The formulation of the simplified analysis techniques is based upon an assumed suitable deformed shape of the structure and limit analysis methods. A rigid-perfectly plastic material is considered. The following formulation differs from classical limit analysis in that large deformations are permitted. The limit pressure so calculated will be denoted as p_0. Usually, there is a little or no difference between the plastic collapse pressure, $p_{2\varepsilon y}$, and the limit pressure, p_0, for rigid or elastic perfectly plastic materials. In these cases, the limit pressure can be employed as a good approximation to the vessel resistance (7,8). In the following discussion, the evaluation of the limit pressure for a stiffened cylinder under uniform internal pressure is presented. Finite element analyses are used to verify the predicted resistance of such structures.

A stiffened cylindrical shell can be considered as a number of rectangular curved panels framed by a ring sector and a stringer section (see Fig. 2). Failure modes for this type of structure can be identified as: (1) General Failure; (2) Inter-ring Failure; and (3) Panel Failure. The first mode is considered to occur when the entire panel expands in the radial direction uniformly as shown in Fig. 3. The inter-ring failure mode occurs when the radial deformation of the

vertical stiffeners and the shell skin increase, while the ring stiffener deformation remains small, i.e., within the elastic range (see Fig. 4). The third failure type occurs when the shell skin bulges outward while the ring and stringer reinforcement remain in the elastic range. For the range of stringer dimension considered herein, the third failure mode is not likely to occur. This will be approximately verified later in this work.

For an axisymmetrically loaded cylindrical shell with large deformation, the membrane strain-displacement relationships are (9):

$$\varepsilon_\phi = \frac{du}{dx} + \frac{1}{2}\left(\frac{dw}{dx}\right)^2 \tag{1}$$

$$\varepsilon_\theta = \frac{w}{r} \tag{2}$$

in which ε_ϕ and ε_θ are the meridional and circumferential membrane strain, respectively, w is the displacement perpendicular to the shell surface; u represents the meridional displacement (see Fig. 2); r is the shell midsurface radius; and x is the cylinder meridional coordinate.

The internal energy, U, dissipated per each panel is written as:

$$U = \int_V (f_\phi \varepsilon_\phi + f_\theta \varepsilon_\theta)\, dv + \int_{V_r} f_r\, \varepsilon_\theta\, dv + \int_{V_s} f_s\, \varepsilon_\phi\, dv \tag{3}$$

where f_ϕ and f_θ are the shell meridional and circumferential membrane stresses, while v represents the material volume. The stresses f_r and f_s, respectively, are the ring and longitudinal stiffener stresses, while v_r and v_s are the ring and longitudinal stiffener volumes, respectively. The energy due to bending strains will be considered as concentrated at plastic hinges.

The external work for a uniform internal pressure loading, p, can be expressed as

$$W = \int_A p\, w\, dA \pm 2\pi r\, (N_\phi\, \bar{u} + M_\phi\, \bar{\theta})\Big|_{\text{boundary}} \tag{4}$$

where A is the surface over which the load is applied. The second term indicates the work of the meridional membrane force N_ϕ and the moment M_ϕ at the plastic hinges at the panel boundaries (N_ϕ and M_ϕ are forces per unit length). The quantity $\bar{u}$ denotes the change in the length of the panel and $\bar{\theta}$ is the slope of the deformed shape at the plastic hinges.

The membrane strains can be written, according to the deformation strain theory of plasticity (6,10), as follows

$$\varepsilon_\phi = C(f_\phi - f_\theta/2) \tag{5}$$

$$\varepsilon_\theta = C\,(f_\theta - f_\phi/2) \tag{6}$$

in which ε_ϕ, ε_θ are the meridional and circumferential strains, respectively, while C denotes a proportionality constant. The von Mises yield criteria (6,10) is employed in this work to relate the membrane stresses to the material yield strength, F_y, as:

$$f_\theta^2 + f_\phi^2 - f_\theta f_\phi = F_y^2 \tag{7}$$

Analysis of the general failure mode

The deformed shape of this mode is illustrated in Fig. 3. For this case, the circumferential strain is assumed to be constant, while the meridional strain is neglected, or

$$\varepsilon_\theta = e \tag{8}$$

$$\varepsilon_\phi = 0 \tag{9}$$

where e is the maximum allowable strain. The plasticity conditions of Eqs. 5 and 7 in conjunction with the assumption in Eq. 9 yields the cylinder stresses as:

$$f_\phi = \frac{1}{\sqrt{3}} F_y \tag{10}$$

$$f_\theta = \frac{2}{\sqrt{3}} F_y \tag{11}$$

In the same way, the ring stresses are found as:

$$f_r = F_y \tag{12}$$

Substitution of the above relationships into Eqs. 3 and 4 results in

$$U = 2\pi r\, s_1 t\, F_y \left(\frac{2}{\sqrt{3}} + \frac{A_1}{s_1 t}\right) e \tag{13}$$

$$W = 2\pi\, r^2\, s_1\, p\, e \tag{14}$$

in which t represents the containment wall thickness and A_1 is the ring stiffener cross-sectional area. Note that the energy dissipated in the stringer and the work done by the membrane forces N_ϕ and M_ϕ (boundary forces) are zero because of the assumed deformed shape. For an elastic-perfectly plastic material, Eq. 13 can be modified as follows. Since the stress strain relationship is linear in the elastic region, the strain energy, U_e, which is accumulated up to yield strain, ε_y, can be approximated as:

$$U_e \simeq \frac{1}{2}\, U\Big|_{e\,=\,\varepsilon_y} \tag{15}$$

Subtracting the complementary elastic energy from the energy given by Eq. 13, the internal energy for an elastic-perfectly plastic material can be approximated as:

$$U = 2\pi\, r\, s_1\, t\, F_y \left(\frac{2}{\sqrt{3}} + \frac{A_1}{s_1 t}\right)\left(e - \frac{1}{2}\,\varepsilon_y\right) \tag{16}$$

When Eqs. 13 or 16 and Eq. 14 are substituted into the following minimization principal relationship

$$\frac{\partial U}{\partial e} - \frac{\partial W}{\partial e} = 0 \tag{17}$$

An expression of the limit pressure, p_o, for the general failure mode is found as:

$$p_o = \frac{t\, F_y}{r}\left(\frac{2}{\sqrt{3}} + \frac{A_1}{s_1 t}\right) \tag{18}$$

Analysis of the inter-ring failure mode

Figure 4 shows the assumed deformed shape of this failure mode. In this case, the circumferential strains are assumed to vary parabolically, while the longitudinal strain is assumed negligible, or

$$\varepsilon_\theta = e\left[1 - \left(\frac{2x}{s_1}\right)^2\right] \tag{19}$$

$$\varepsilon_{\phi} = 0 \tag{20}$$

where e represents the circumferential strain midway between the rings, i.e., at x equal zero. With the strain displacement relation given in Eqs. 1 and 2, the radial and meridional displacements, w and u, respectively, for this failure mode are:

$$w = er\left[1 - \left(\frac{2x}{s_1}\right)^2\right] \tag{21}$$

$$u = -\frac{32\, e^2 r^2\, x^3}{s_1^4} \tag{22}$$

Plastic hinges are assumed to form at the upper and lower boundaries of the panel. The rotation, $\bar{\theta}$, is given by

$$\bar{\theta} = \left.\frac{dw}{dx}\right|_{x = \pm \frac{s_1}{2}} = \pm \frac{4\, er}{s_1} \tag{23}$$

The change in the panel length, $\bar{u}$, calculated using Eq. 22, is

$$\bar{u} = \frac{4e^2 r^2}{3\, s_1} \tag{24}$$

Substituting Eqs. 10, 11, 19, 20, 21 and 23 into Eqs. 3 and 4 results in the following energy and work relationships

$$U = \frac{8 \pi rte\, s_1 F_y}{3\sqrt{3}} \tag{25}$$

for a rigid-perfectly plastic material. Following the discussion mentioned in the preceding section, the dissipated energy for an elastic-perfectly plastic material can be approximated as:

$$U = \frac{8\pi rt\, s_1 F_y}{3\sqrt{3}} (e - \frac{1}{2}\varepsilon_y) \tag{26}$$

The external work, W, given in Eq. 4 becomes

$$W = \frac{4\pi r^2 e}{3} (s_1 p - \frac{4 r e N_\phi}{s_1} - \frac{12 M_\phi}{s_1}) \tag{27}$$

Equilibrium in the vertical direction results in

$$N_\phi = \frac{Pr}{2} \tag{28}$$

The effect of the axial force, N_ϕ, on the section plastic moment capacity, M_ϕ, is illustrated in Fig. 5. The yield value of N_ϕ is expressed as:

$$N_y = F_y t \left(1 + \frac{A_2}{s_2 t}\right) \tag{29}$$

where A_2 and s_2 are the stringer cross-sectional area and spacing, respectively. Since N_ϕ/N_y is of the order of $1/\sqrt{3}$ (see Eq. 10), the effect of the axial force on the plastic moment capacity of a stringer stiffened cylinder can be assumed insignificant (see Fig. 5). For an unstiffened cylinder, the last term in Eq. 27 is quite small and hence the variation of the plastic moment will not significantly affect the limit pressure. With this in mind, the moment at the plastic hinges will be taken equal to the full plastic moment, M_p, i.e.,

$$M_\phi = M_p \tag{30}$$

where M_p is written as:

$$M_p = Z F_y \tag{31}$$

in which Z is the plastic section modulus of the shell and stringer per unit circumference and is calculated with respect to the shell middle surface as:

$$Z = \frac{t^2}{4} + \frac{A_2 c}{s_2} \tag{32}$$

where c denotes the eccentricity of the stringer centroid measured from the shell middle surface.

Substituting Eqs. 28 and 31 into Eq. 26 and using the relation given in Eq. 17 yields

$$p_o\left(1 - \frac{4\, e\, r^2}{s_1^2}\right) = \frac{F_y\, t}{r}\left(\frac{2}{\sqrt{3}} + \frac{12\, Z\, r}{t\, s_1^2}\right) \tag{33}$$

where e is the circumferential membrane strain midway between rings. The strain e is taken as:

$$e = 2\, \varepsilon_y \tag{34}$$

which corresponds to a strain ductility capacity of two. Introducing Eq. 34 into Eq. 33 gives a limit pressure for the inter-ring mode as:

$$p_o = \frac{F_y t/r}{\left(1 - \frac{8\, \varepsilon_y r^2}{s_1^2}\right)}\left(\frac{2}{\sqrt{3}} + \frac{12\, Zr}{s_1^2\, t}\right) \tag{35}$$

Notice that the parenthetical term in the denominator represents the effect of large deformations. This term would be one for small displacement limit pressures.

Calibration of the Simplified Methods

Before proceeding to the application of the foregoing approximate analyses, it is appropriate to verify the validity of the methods. Since several assumptions are typically involved in the formulation and analysis of the proposed approaches, they will be verified by comparing the results to finite elements.

The ANSYS (11) finite element computer program was used in this study to perform the finite element analysis. Material and geometric nonlinearities were considered in the analysis. Material nonlinearly was included in the analysis using what is called classical bilinear kinematic hardening option in the ANSYS program. An elastic perfectly plastic material was used. A convergence criterion on plastic strain increment/elastic strain of 0.1 was employed. Geometric nonlinearity effects were treated using the stress stiffening option provided in the program. Reference 12 concludes that this option adequately accounts for large displacement effects for axisymmetric shells under uniform static pressure. The axisymmetric structure was modeled by a number of isoparametric quadrilateral eight node elements (four corner and four midside nodes). This element is referred to as STIF 82 in the ANSYS element library. An element length of about $\sqrt{rt}/2$ was used. The reader is referred to Ref. (12) for an extensive study and a comparison of the results when using different element size and analysis options.

In the following, each of the three previously defined failure modes is studied individually. The nonaxisymmetric behavior which results from the presence of the longitudinal reinforcement was exam-

ined first. One typical panel (see Fig. 2) of the shell skin with the framing stiffeners was analyzed. The cylinder has an r/t ratio of 1200; the ring and longitudinal stiffeners are spaced at 250 inches and 6 degrees, respectively. The circumferential and stringer areas were selected such that

$$\alpha_1 = \frac{A_1}{s_1 t} = 0.2 \tag{36}$$

$$\alpha_2 = \frac{A_2}{s_2 t} = 0.2 \tag{37}$$

These areas and spacings were chosen as upper practical limits for containment vessels to increase the likelihood of a panel failure mode.

The finite element three-dimensional solution was accomplished using a triangular shell element (six degrees of freedom per node). Only one-quarter of the panel need be analyzed because of the panel symmetry conditions (see Fig. 6).

An axisymmetric approximation to this panel was also analyzed by finite element methods. The cylindrical shell and ring stiffeners were modeled using the isoparametric axisymmetric solid elements, while a beam element was used to idealize the stringer (see Fig. 7). The cylinder and stringer were connected using linear constraint equations which simulate a rigid connection.

Figure 8 contains plots of internal radial pressure versus radial displacement at locations 1, 2, 3 and 4 of the three-dimensional model (Fig. 6). Radial displacements at Points 5 and 6 of Fig. 7 are also shown in Fig. 8. The pressure-displacement relationship of Points 3 and 4 coincides very closely with that of Point 6 (axisymmetric model). Although the difference between radial displacements of Points 1 and 2 is noticeable in the linear portion, there is little difference in the non-linear range (near the plastic pressure). Moreover, the radial displacement of Point 5 (from the approximate axisymmetric finite element model) is close to that of Points 1 and 2 for the more analytically correct three-dimensional analysis. In the nonlinear range, those two curves are almost the same. Since there is little difference in the radial displacement predicted by the three-dimensional and the axisymmetric analysis of the same panel, the axisymmetric finite element idealization will be used throughout the remainder of this study. In other words, the circumferential variation of the displacement and stress is not significant and can be neglected for this range of structural parameters. Large savings in computer time will result from this finding. Additionally, since the circumferential variation in displacement is small, the bulging panel failure mode defined previously cannot occur for this range of geometrics, i.e., for stringers spaced at less than 6 degrees and α_2 (Eq. 37) less than 0.2.

The other two possible failure modes, i.e., the general and interring modes, were also examined. A total of six models with different geometric parameters were used for each mode. The geometric parameters

employed for each model are tabulated in Tables 1 and 2 for the general and the inter-ring failure modes, respectively. Pressure versus maximum circumferential membrane strain was predicted and $p_{2\varepsilon y}$ was evaluated at twice the elastic strain.

Figures 9 and 10 show the pressure strain curves for the A, B and C models as a sample for the general and inter-ring failure modes, respectively. The calculated plastic pressure, $p_{2\varepsilon y}$, for those two modes are given in Tables 1 and 2. The limit pressure p_0 predicted using Eqs. 18 and 35 for the general and the inter-ring failure modes, respectively, is also tabulated.

The calculated limit pressure is in agreement with that found using the finite element analysis. The longitudinal stiffener does not have a significant effect on the calculated plastic pressure when failure is caused by yielding of the rings (compare Model A versus B and Eq. 18). Also, in the general failure mode, and for a constant α_1, the ring spacing has little effect on the predicted plastic pressure as illustrated by Models C versus D and that predicted by Eq. 18. The finite element results for the inter-ring failure mode indicated that the shell and stringer elements midway between the rings were stressed uniformly at yield, while the stringer stress is rectangularly distributed at the rings. In other words, bending stresses are significant at the circumferential stiffeners. Figure 11 illustrates the deformed shape of Model A at a pressure of 80 psi (.55 MN/m^2). The figure shows that the slope is continuous midway between the rings and that a slope discontinuity occurs at the rings. From these observations, it can be

concluded that there is a circumferential plastic hinge which forms at each ring elevation while there is zero bending energy midway between the rings. One can also see the resemblance between the deformed shape in Fig. 11 and the deformed shape given by Eq. 21.

Limit Pressure for Other Shell Structures

Stiffened conical shell

The development of the simplified methods for stiffened conical shells is similar to that for the stiffened cylinder. Formulas for the prediction of the limit pressure are listed herein. The derivations of these equations are given in the Appendix. For the general failure mode type (rings and shell plating yield), the limit pressure is given as:

$$p_o = \frac{t F_y/r}{(1 + \frac{\rho_1^2}{12})} (\frac{2}{\sqrt{3}} + \frac{\alpha_1 r_r}{r}) \tag{38}$$

where

$$r = \frac{r_1 + r_2}{2 \sin\phi} \tag{39}$$

$$\rho_1 = \frac{r_2 - r_1}{r \sin\phi} \tag{40}$$

in which r_1 and r_2 are the upper and lower radii of the cone segment, respectively (see Fig. 12), r_r is the ring radius and ϕ is the slope of the shell meridian line.

The limit pressure for the inter-ring failure mode is given as

$$p_o = \frac{F_y \, t/r \quad (\frac{2}{\sqrt{3}} + \frac{12 \, \bar{Z} \, r}{t \, L^2})}{1 + \frac{\rho_1^2}{20} - 8 \, \varepsilon_y \, \rho_2^2 (1 + \frac{3}{20} \rho_1^2 + \frac{3}{8} \rho_3^2)} \tag{41}$$

where

$$\rho_2 = \frac{\sqrt{(r_1^2 + r_2^2)/2}}{s_1} \tag{42}$$

$$\rho_3 = \frac{r_2 - r_1}{\sqrt{(r_1^2 + r_2^2)/2}} \tag{43}$$

$$\bar{Z} = \frac{Z_1 \, r_2^2 + Z_2 \, r_1^2}{(r_1 + r_2)^2} \tag{44}$$

in which L is the ring spacing measured in the meridional direction. r_1 and r_2 are the shell segment radii as shown in Fig. 13. The plastic section moduli per unit circumferential length at the top and bottom boundaries are Z_1 and Z_2, respectively. Note that the equations of the

stiffened conical shell specialize to the cylindrical case discussed early in this study.

Containment vessel heads

The following section focuses on the evaluation of the containment head resistance subjected to uniform internal static pressure. Numerous studies (7, 9, 13, 14, 15) have been conducted to investigate the strength of different head types. A brief summary of this work is presented herein.

Hemispherical heads The limit pressure for a hemispherical shell is obtained as

$$p_o = \frac{2 F_y t}{r} \tag{45}$$

2:1 Ellipsoidal heads The following section summarizes the study conducted by Galletly and Aylward (13). Failure of ellipsoidal heads can occur by two possible failure modes: (1) elastic or elastic-plastic buckling; or (2) plastic collapse failure. In the first failure mode, wrinkles or lobes form around the circumference of the shell in the vicinity of the knuckle. The asymmetric buckling is caused by circumferential compressive stresses induced in the shell by inward displacement in the knuckle vicinity (13). In the plastic collapse mode, an axisymmetric limit mechanism is formed with accompanying large displacement. This mode provides a limit pressure similar to that dis-

cussed early in this work. The resistance of these two failure modes are given in Ref. (13) as:

$$p_{cr} = 10.4\ F_y\ (\frac{t}{2r})^{1.25} \tag{46}$$

for the elastic-plastic asymmetric buckling, and

$$p_o = \frac{F_y t}{r}\ (1 + 50\ \varepsilon_y) \tag{47}$$

for the axisymmetric plastic collapse mode. Limits on the above equation are:

$$30\ \text{ksi}\ (207\ \text{MN/m}^2) < F_y < 60\ \text{ksi}\ (414\ \text{MN/m}^2) \tag{48}$$

$$250 < r/t < 750 \tag{49}$$

Torispherical heads Failure of torispherical heads can also occur by asymmetric buckling in the knuckle region or by plastic collapse. References 14 and 15 give equations for each of these possible failure modes. For the asymmetric buckling mode, the resistance is given as:

$$p_{cr} = \frac{285\ F_y\ (1\text{-}125\ \varepsilon_y)(r_t/2r)^{0.84}}{(\frac{2r}{t})^{1.53}\quad (\frac{R_s}{2r})^{1.1}} \tag{50}$$

$$p_o = \frac{12.6\ F_y\ (1 + 240\ \varepsilon_y)(r_t/2r)^{1.04}}{(\frac{2r}{t})^{1.09}\quad (\frac{R_s}{2r})^{a}} \tag{51}$$

where

$$a = \begin{cases} 0.79 & \frac{R_s}{2r} > 1 \\ 1.10 & \frac{R_s}{2r} < 1 \end{cases} \tag{52}$$

in which r_t and R_s are the toroidal (knuckle) and spherical (crown) radii of the torisphere, respectively. The limits of the above equations are:

$$20 \text{ ksi } (138 \text{ MN/m}^2) < F_y < 75 \text{ ksi } (517.5 \text{ MN/m}^2) \tag{53}$$

$$250 < \frac{r}{t} < 750 \tag{54}$$

$$0.06 < \frac{r_t}{2r} < 0.18 \tag{55}$$

$$0.75 < \frac{R_s}{2r} < 1.5 \tag{56}$$

Applications

To demonstrate the use of the methods, the containment vessel shown in Fig. 14 was analyzed. This containment is fairly typical. The containment consists of several simple axisymmetric sections placed together. A torispherical head with toroidal and spherical radii of 5.42 ft. (1.65 m) and 28.67 ft. (8.74 m), respectively, was used to cover the containment. In addition, part of the containment is circumferentially and longitudinally stiffened as shown in Fig. 14. The containment resistance was analyzed twice: (1) with the ANSYS finite element program and (2) with the simplified approaches presented herein.

The containment shell and the ring stiffeners were modeled for the finite element using axisymmetric solid elements. Beam elements were employed to idealize the longitudinal stiffeners. The shell-stringer connection was modeled by relating the displacement of the vessel nodes to those of the stiffeners with constraint equations. No element size in the shell exceeds $\sqrt{rt}/2$. Also, the nodes along the containment base were completely restrained. A material yield strength of 41.8 ksi (288.42 MN/m^2) and modulus of elasticity of 29,000 ksi (200,100 MN/m^2) were used. The uniform internal pressure was increased in even steps of 20 psi (0.138 MN/m^2) until a pressure of 100 psi (0.690 MN/m^2) was reached. The size of the load step was then reduced to obtain convergence of the nonlinear solution. The solution was continued until a pressure of 134 psi (0.925 MN/m^2) was reached. At this point, the maximum circumferential membrane strain reached twice the yield strain,

i.e., a ductility factor of two. The resulting pressure-strain, pressure-displacement and deformed shape are shown in Figs. 15, 16 and 17, respectively. The maximum radial displacement and hoop strain occurred in the unstiffened portion of the lower cylindrical section as illustrated in Fig. 17. The containment resistance, $p_{2\epsilon y}$, is predicted as 134 psi (0.925 MN/cm^2). For the reader's interest, the total computer (CDC 7600) time for the solution was 2950 cpu seconds.

The simplified methods outlined previously were also used to predict the limit pressure for the containment vessel in Fig. 14. More specifically, Eqs. 18, 35, 38, 41, 50 and 51 were employed to analyze the possible thirty failure modes. Minimum containment wall thicknesses were used when shell thickness varied within the region of the failure mode. From the results given in Table 3, the containment resistance based on the simplified analysis is 133 psi (0.918 MN/m^2). Also, the controlling failure mode occurred in the stringer stiffened portion of the lower cylindrical section (Region 14). This resistance was predicted using Eq. 35 considering a stringer stiffened cylinder with a length of 397 in. (10.08 m).

Conclusions

Simplified approaches were developed for the analysis of stiffened axisymmetric shells under uniform static internal pressure. The methods are based on classical limit analysis theory and take into account the effects of large deformations. Finite element techniques were used to guide the formulation of these methods. Twelve axisymmetric models

were analyzed using the finite element technique and simplified approaches. An actual containment vessel analysis is also presented to illustrate the applicability of the methods. For a static uniform internal pressure, the simplified methods give good results when applied to axisymmetric stiffened shells. The methods are sufficiently accurate to define the limit pressure of such structures. These approaches provide the limit pressure for each possible failure mode. This would clearly be excessively expensive to predict by the finite element technique, which typically yields only the mode with the minimum resistance. (Reliability analysis techniques usually require the prediction of all failure modes.)

Appendix. Simplified Analysis of Stiffened Conical Shells

The development of the simplified methods for stiffened conical shells is closely parallel to that of stiffened cylinders. For a conical surface, the strain displacement relationships, Eqs. 1 and 2, specialize to

$$\varepsilon_\theta = \frac{u}{x} + \frac{w}{x} \tan\phi \qquad \text{(A-1)}$$

$$\varepsilon_\phi = \frac{du}{dx} + \frac{1}{2} \left(\frac{dw}{dx}\right)^2 \qquad \text{(A-2)}$$

where u, w, x and ϕ are shown in Fig. 12.

Analysis of the general failure mode

The deformed shape of this mode is shown in Fig. 12. For this mode, the circumferential and meridional strains are taken as:

$$\varepsilon_\phi = 0 \tag{A-3}$$

$$\varepsilon_\theta = e \tag{A-4}$$

Substituting Eqs. A-3 and A-4 into Eqs. A-1 and A-2 yields the following displacements

$$w = \frac{e\ x}{\tan\phi} \tag{A-5}$$

$$u = \frac{e^2}{2\ \tan^2\phi}\ (x_2 - x) \tag{A-6}$$

in which x_2 is the distance measured from the cone apex to the lower edge of the cone segment (see Fig. 12). Note that the term dw/dx has been neglected with respect to $\tan\phi$ in Eq. A-5.

The internal energy, U, dissipated per each panel, can be written as:

$$U = \int_v f_\theta \varepsilon_\theta\ dv + n_r \int_{v_r} f_r\ \varepsilon_\theta\ dv \tag{A-7}$$

where n_r is the number of the ring stiffeners within the panel. No energy is stored in the stringers for this mode. The shell circumfer-

ential stresses, f_θ, and the ring stresses, f_r, are those as given in Eqs. 11 and 12, respectively.

The external work for a uniform internal pressure can be written as:

$$W = \int_A p\, w\, dA \pm 2\, \pi r_1 N_\phi \bar{u} \Big|_{\text{boundary}} \tag{A-8}$$

in which $\bar{u}$ represents the change in the inclined length of the cone segment, L, and is expressed as:

$$\bar{u} = -\frac{e^2 L}{2 \tan^2\phi} \tag{A-9}$$

Note that there is no bending energy considered in this failure mode. Substituting the necessary equations into Eqs. A-7 and A-8 and using the minimization principle given in Eq. 17 yields the resistance of the general failure mode of a stiffened conical shell as:

$$p_o = \frac{t F_{y/r} \left(\frac{2}{\sqrt{3}} + \frac{\alpha_1 r_r}{r}\right)}{\left(1 + \frac{\rho_1^2}{12} - \frac{e}{2 \tan^2\phi}\right)} \tag{A-10}$$

where

$$r = \frac{r_1 + r_2}{2 \sin\phi} \tag{A-11}$$

$$\rho_1 = \frac{r_2 - r_1}{r \sin\phi} \tag{A-12}$$

$$\alpha_1 = \frac{A_1}{st} \tag{A-13}$$

in which r_r is the ring radius (see Fig. 12). The effect of the strain, e, in the denominator of Eq. A-10 can be neglected, particularly when the angle ϕ is greater than 45°. This is most likely the case for containment vessels. Omitting this term, Eq. A-10 becomes

$$p_o = \frac{t F_{y/r}}{(1 + \frac{\rho_1^2}{12})} (\frac{2}{\sqrt{3}} + \frac{\alpha_1 r_r}{r}) \tag{A-14}$$

Analysis of inter-ring failure mode

For the inter-ring failure mode, the displacement of the ring is considered negligible in comparison to that of the shell skin. Figure 13 shows the assumed deformed shape of the inter-ring failure mode. In this case, the circumferential membrane strain is assumed to vary parabolically and the meridional strain is assumed negligible, or

$$\varepsilon_\theta = e \left[1 - (\frac{2x'}{L})^2\right] \tag{A-15}$$

$$\varepsilon_\phi = 0 \tag{A-16}$$

in which x' is measured from the center of the segment (Fig. 13), and is written as:

$$x' = x - r \tan\phi \tag{A-17}$$

Integration of the strain-displacement relationship in Eqs. A-1 and A-2 yields the following displacements:

$$w = \frac{e}{\tan\phi}\left[1 - \left(\frac{2x'}{L}\right)^2\right](x' + r\tan\phi) \tag{A-18}$$

$$\frac{du}{dx} = -\frac{e^2}{2\tan\phi}\left[1 - \frac{8\,x'\,r\tan\phi}{L^2} - \frac{12\,x'^2}{L^2}\right] \tag{A-19}$$

The term, dw/dx, has been neglected with respect to $\tan\phi$ in the above development. Equation A-19 can be integrated to give the changes in the upper and lower halves of the cone segment length. These changes are written as;

$$\bar{u}_2, \bar{u}_1 = \mp\frac{1}{2}e^2 L\left[\pm\frac{2}{5}\cot^2\phi + \frac{r\cot\phi}{L} \pm \frac{8\,r^2}{3\,L^2}\right] \tag{A-20}$$

where the subscripts 1 and 2 are used for the upper and lower halves of the cone segment, respectively. The rotation of the plastic hinges at the upper and lower boundaries, respectively, are:

$$\bar{\theta}_1 = \frac{4\ e\ r_1}{s_1} \tag{A-21}$$

$$\bar{\theta}_2 = \frac{-4\ e\ r_2}{s_2} \tag{A-22}$$

The moments at the plastic hinges are taken as the full plastic moment (Eqs. 30 and 31), M_{p_1} and M_{p_2}. Also, for uniform internal pressure, the meridional membrane forces at the upper and lower boundaries, respectively, are:

$$N_{\phi_1} = \frac{p\ r_1}{2\ \sin\phi_1} \tag{A-23}$$

$$N_{\phi_2} = \frac{p\ r_2}{2\ \sin\phi_2} \tag{A-24}$$

The internal membrane energy for this failure mode is written as:

$$U = \int_v f_\theta\ \varepsilon_\theta\ dv \tag{A-25}$$

where v represents the shell plate volume. The external work can be expressed as follows:

$$W = \int_A pwdA \pm 2\pi[r_1(N_{\phi_1}\bar{u}_1+M_{p_1}\bar{\theta}_1)+r_2(N_{\phi_2}\bar{u}_2+M_{p_2}\bar{\theta}_2)]\Big|_{boundary} \tag{A-26}$$

Substituting Eqs. A-15 through A-24 into Eqs. A-25 and A-26 and recalling the minimization principle given by Eq. 17 results in the following limit pressure for the inter-ring failure mode.

$$p_o = \frac{F_y \, t/r \quad \left(\frac{2}{\sqrt{3}} + \frac{12 \, \bar{Z} \, r_1}{t \, L^2} \right)}{1 + \frac{\rho_1^2}{20} - 8 \, \varepsilon_y \, \rho_2^2 \left(1 + \frac{3}{20} \rho_1^2 + \frac{3}{8} \rho_3^2\right)} \tag{A-27}$$

in which ε_y is the material yield strain and

$$\rho_2 = \frac{\sqrt{(r_1^2 + r_2^2)/2}}{s_1} \tag{A-28}$$

$$\rho_3 = \frac{r_2 - r_1}{\sqrt{(r_1^2 + r_2^2)/2}} \tag{A-29}$$

$$\bar{Z} = \frac{Z_1 \, r_2^2 + Z_2 \, r_1^2}{(r_1 + r_2)^2} \tag{A-30}$$

List of Symbols

The following symbols are used in this part:

A = area over which the load is applied;

A_1 = ring stiffener cross-sectional area;

A_2 = longitudinal stiffener cross-sectional area;

c = eccentricity of the longitudinal stiffener centroid;

C = proportionality constant;

e = mechanism strain;

f_θ, f_ϕ = circumferential an meridional stresses, respectively;

F_y = material yield strength;

L = meridional ring spacing;

M_ϕ = moment per unit length;

M_p = section plastic moment capacity per unit length;

N_ϕ = axial force per unit length;

$p_{2\varepsilon y}$ = plastic collapse pressure;

p_o = limit pressure;

r = radius;

R_s = radius of spherical portion of torisphere;

r_t = radius of toroidal portion of torisphere;

s_1 = ring stiffener spacing;

s_2 = longitudinal stiffener spacing;

t = thickness;

u = meridional displacement;

$\bar{u}$ = change in the shell meridional length;

U = internal strain energy;

U_e = internal elastic strain energy;

w = displacement perpendicular to shell surface;

W = external energy;

Z = section plastic modulus per unit length;

σ_r, σ_s = ring and stringer stresses, respectively;

$\varepsilon_\theta, \varepsilon_\phi$ = circumferential and meridional strains, respectively;

$\bar{\theta}$ = slope of the deformed shell;

ρ_1, ρ_2, ρ_3 = constants dependent upon conical shell geometric parameters.

References

1. Paul, B. and Hodge, P. G., Jr. "Carrying Capacity of Elastic-Plastic Shells under Hydrostatic Pressure." Proceedings of the 3rd U.S. National Congress of Applied Mechanics, 631 (1958).

2. Onat, E. T. "The Plastic Collapse of Cylindrical Shells under Axially Symmetrical Loading." Quarterly of Applied Mathematics, 13 (1955): 63.

3. Hodge, P. G., Jr. and Panarelli, J. "Interaction Curves for Circular Cylindrical Shells According to the von Mises or Tresca Yield Criteria." Journal of Applied Mechanics, 29 (June 1962): 375-380.

4. Hodge, P. G., Jr. "Plastic Design of a Closed Cylindrical Structure." Journal of Mechanics and Physics of Solids, 12 (1964): 1-10.

5. Biron, A. and Sawczuk, A. "Plastic Analysis of Rib Reinforced Cylindrical Shells." Transactions of the ASME, Journal of Applied Mechanics, 89, Series E (March 1967): 37-42.

6. Save, M. A. and Massanet, C. E. Plastic Analysis and Design of Plates, Shells and Disks." Amsterdam:North Holland, 1972.

7. Gerdeen, J. C. "A Critical Evaluation of Plastic Behavior Data and a Unified Definition of Plastic Loads for Pressure Components." Draft of Final Report submitted to Pressure Vessel and Research Committee, Welding Research Council (April 1979).

8. Greimann, L. F., Fanous, F. S., Wolde-Tinsae, A., Ketelaar, D., Lin, T. and Bluhm, D. "Reliability Analysis of Containment Strength." Report to U.S. NRC, NUREG/CR-2442, IS-4753 (Nov. 1981).

9. Baker, E.H., Cappel, A.P., Kovalevsky, L. and Verehe, R. M. Shell Analysis Manual. Springfield, Virginia:NASA CR-912, Clearinghouse for Federal Scientific and Technical Information, N68-24802, 1968.

10. Ford, H. and Alexander, J. M. Advanced Mechanics of Materials. 2nd ed. New York:John Wiley and Sons, Inc., 1963.

11. ANSYS, Engineering Analysis System. User's Manual. Houston, Pa.:Swanson Analysis System, Inc., 1979.

12. Greimann, L. F., Fanous, F. S., Sabri, A., Ketelaar, D., Wolde-Tinsae, A. and Bluhm, D. "Reliability Analysis of Containment Strength." Report to U.S. NRC, NUREG/CR-1981, IS-47353 (Nov. 1980).

13. Galletly, G. D. and Aylward, R. N. "Plastic Collapse and Controlling Failure Pressure of Thin 2:1 Ellipsoidal Shells Subjected to Internal Pressure." Journal of Pressure Vessel Technology, 101 (Feb. 1979), 64-72.

14. Randamohan, S. K. and Galletly, G. D. "Plastic Collapse of Thin Internally Pressurized Torispherical Shells." Journal of Pressure Vessel Technology, 101 (Nov. 1979), 311-370.

15. Galletly, G. D. and Randamohan, S. K. "Elastic-Plastic Buckling of Internally Pressurized Thin Torispherical Shells." Journal of Pressure Vessel Technology, 101 (Aug. 1979), 216-225.

Table 1. Geometric parameters - theoretical plastic pressure and limit pressure for general failure mode models

Model	r/t	α_1	α_2	s_1/r	Stringer Spacing (degrees)	Plastic Pressure $p_{2\varepsilon y}$(psi)	Limit Pressure p_o(psi)
A	1200	1	0.2	0.125	6	92	90
B	1200	1	--	0.125	6	87	90
C	1200	0.2	--	0.25	6	60	57
D	1200	0.2	--	0.25	6	61	57
E	600	0.2	--	0.125	6	120	113
F	600	1	--	0.125	6	178	178

Table 2. Geometric parameters - theoretical plastic pressure and limit pressure for inter-ring failure mode models

Model	r/t	α_1	α_2	s_1/r	Stringer Spacing (degrees)	Plastic Pressure $p_{2\varepsilon y}$(psi)	Limit Pressure p_o(psi)
A	1200	1	0.1	0.25	6	69	72
B	1200	rigid	0.1	0.25	6	73	72
C	1200	rigid	0.1	0.375	6	57	57
D	1200	1	0.2	0.25	6	78	80
E	1200	1	0.0	0.25	6	62	64
F	600	1	0.0	0.25	6	125	130

Table 3. Containment vessel individual failure mode resistance

Failure[a] Mode	Limit Pressure (psi)	Failure Mode #	Limit Pressure (psi)
1	812	16	143
2	---[b]	17	202
3	273	18	176
4	---[b]	19	226
5	268	20	186
6	---[b]	21	168
7	273	22	160
8	---[b]	23	201
9	264	24	177
10	---[b]	25	818
26	251	26	883
12	---[b]	27	483
13	147	28	209
14	133	29	255
15	150	30	183

NOTE: 1 in. = 2.54 cm.; 1 psi = 0.006895 MN/m^2.

[a]Failure modes #1,3,5,..27 are general failure modes; failure modes #2,4,6,..28 are inter-ring failure modes; failure modes #29 and 30, respectively, are buckling and plastic collapse modes of the torispherical head.

[b]Improbable failure mode; denominator is negative in Eq. 35.

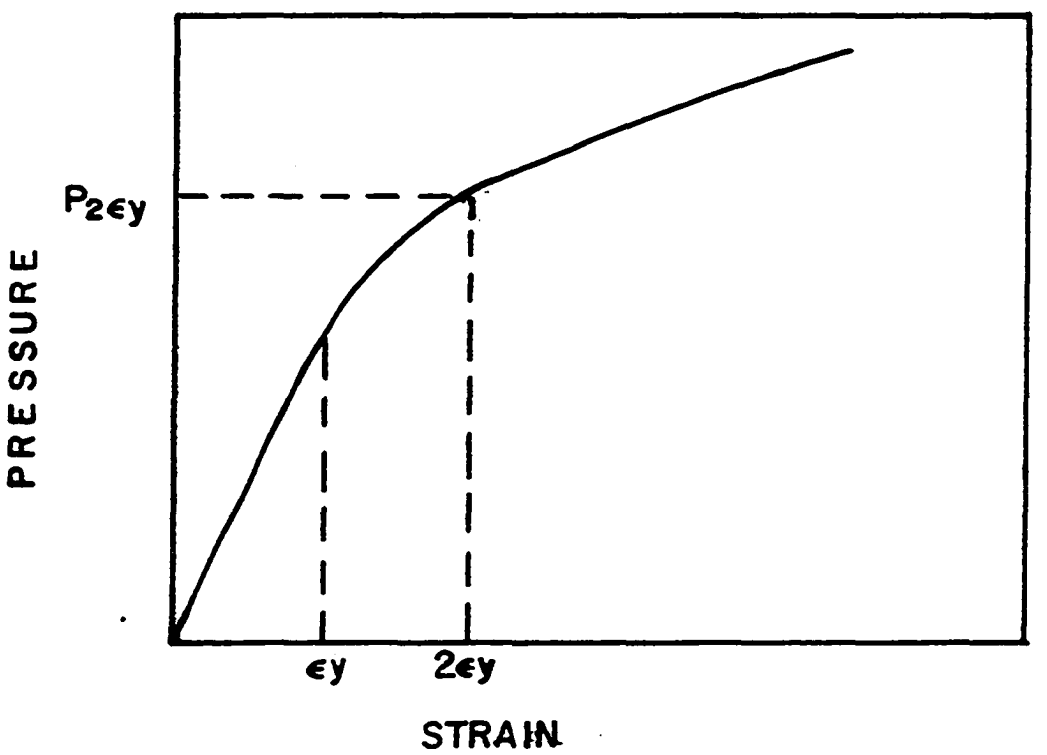

Figure 1. Uniform static pressure failure criteria

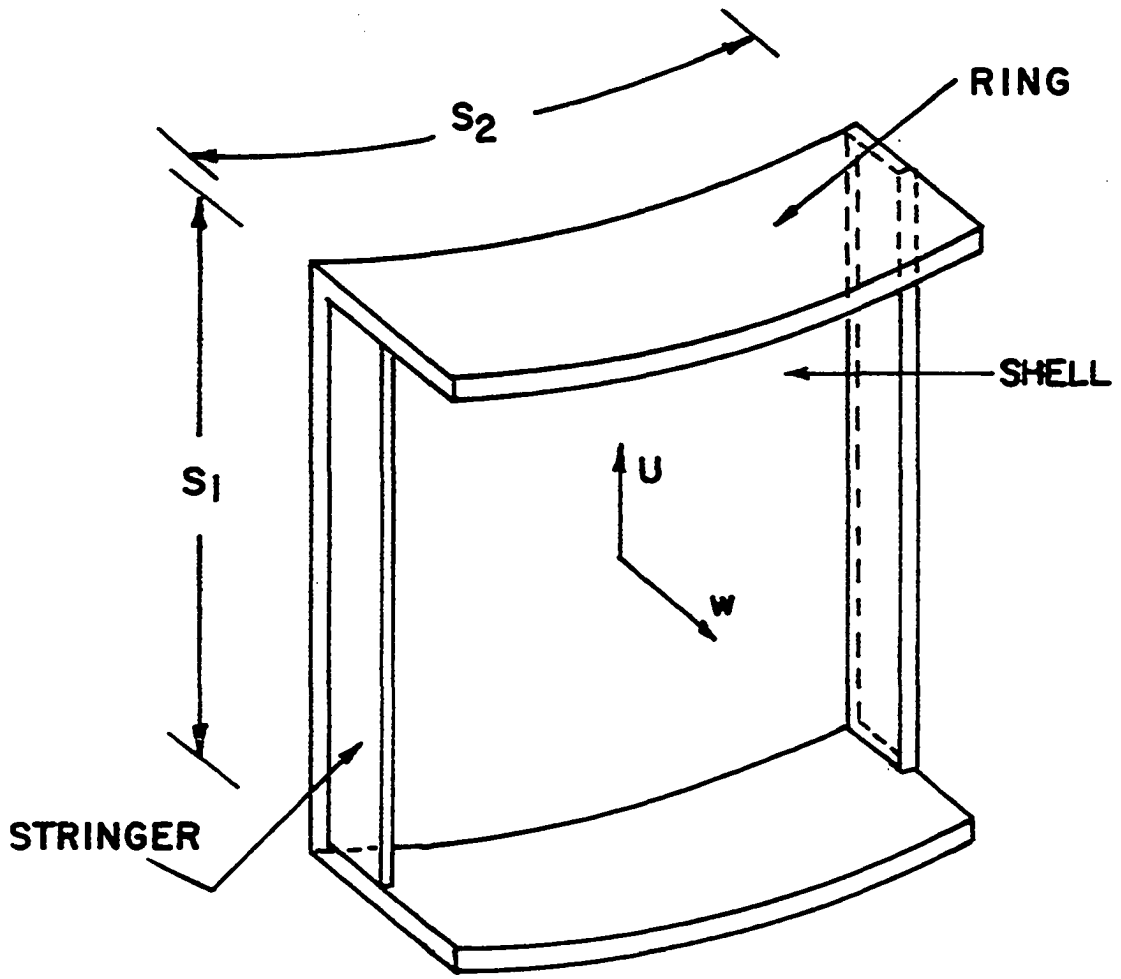

Figure 2. Typical stiffened shell panel

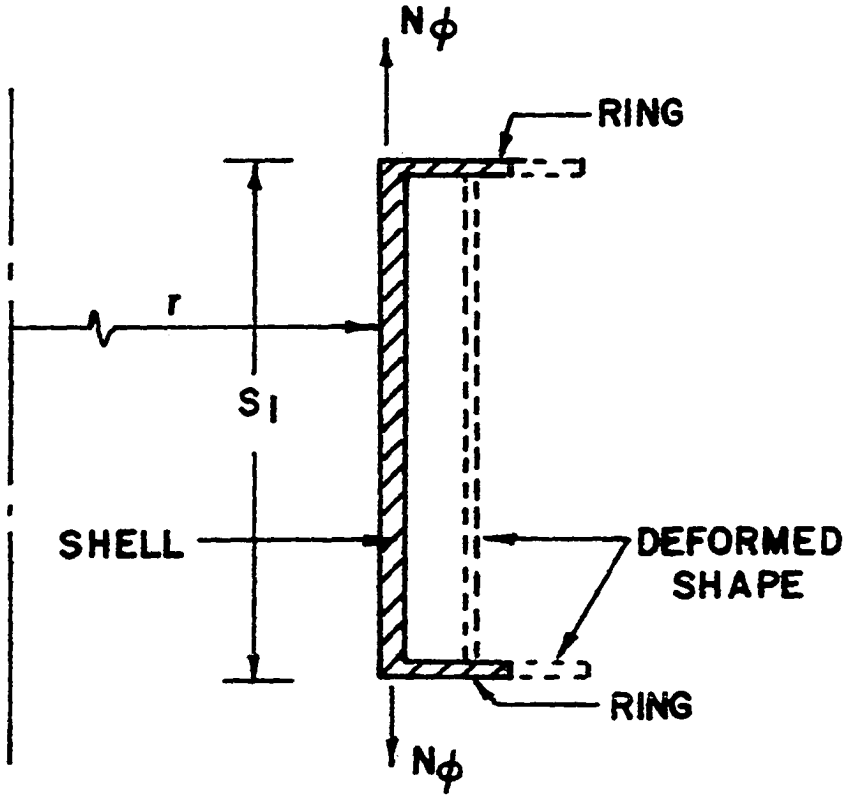

Figure 3. Deformed shape - general failure mode
(stringer not shown)

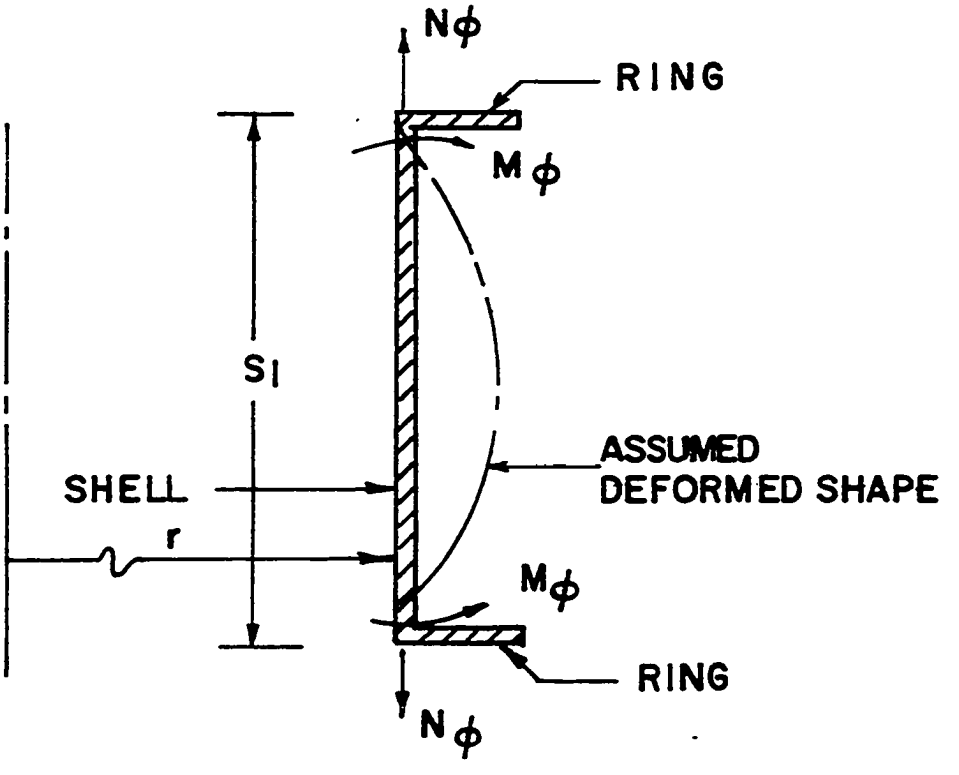

Figure 4. Deformed shape - inter-ring failure mode (stringer not shown).

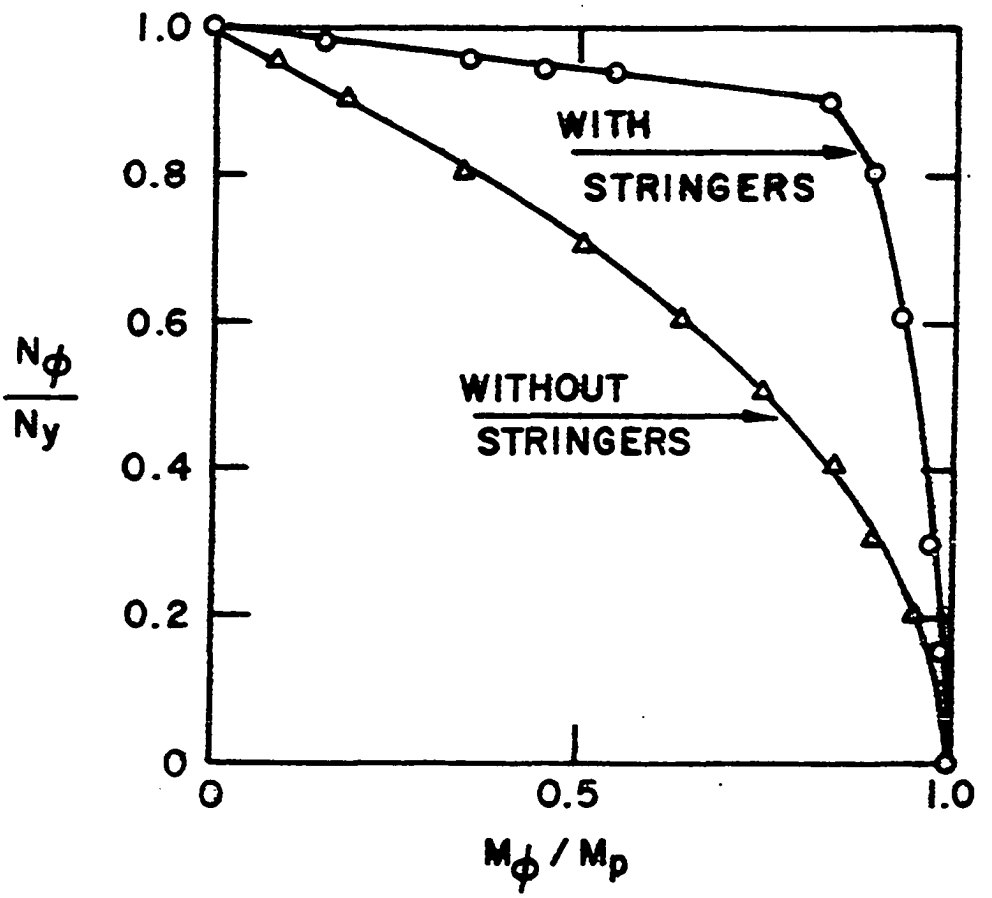

Figure 5. Interaction diagram for plastic moment capacity

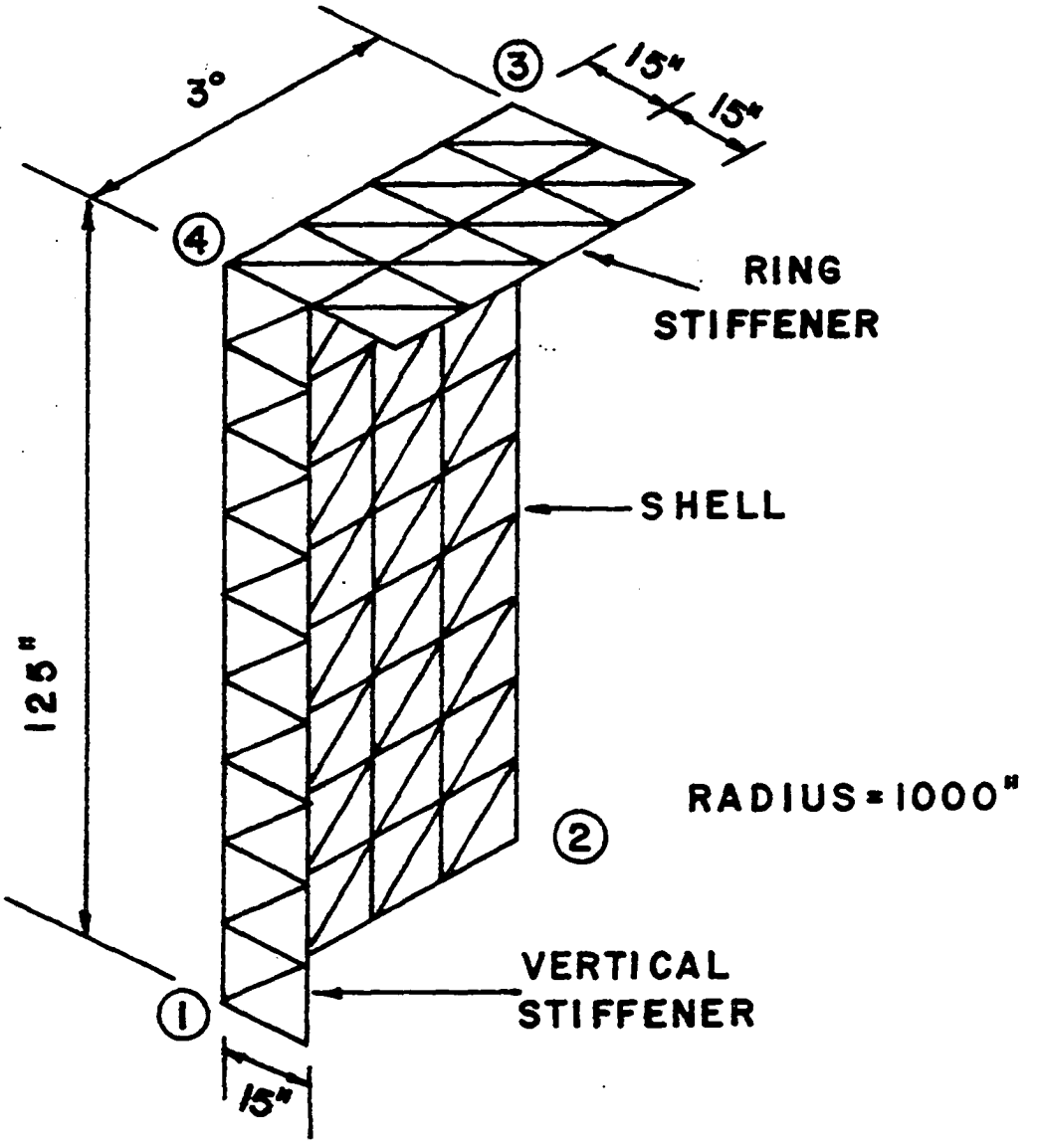

Figure 6. Finite element mesh - three-dimensional idealization

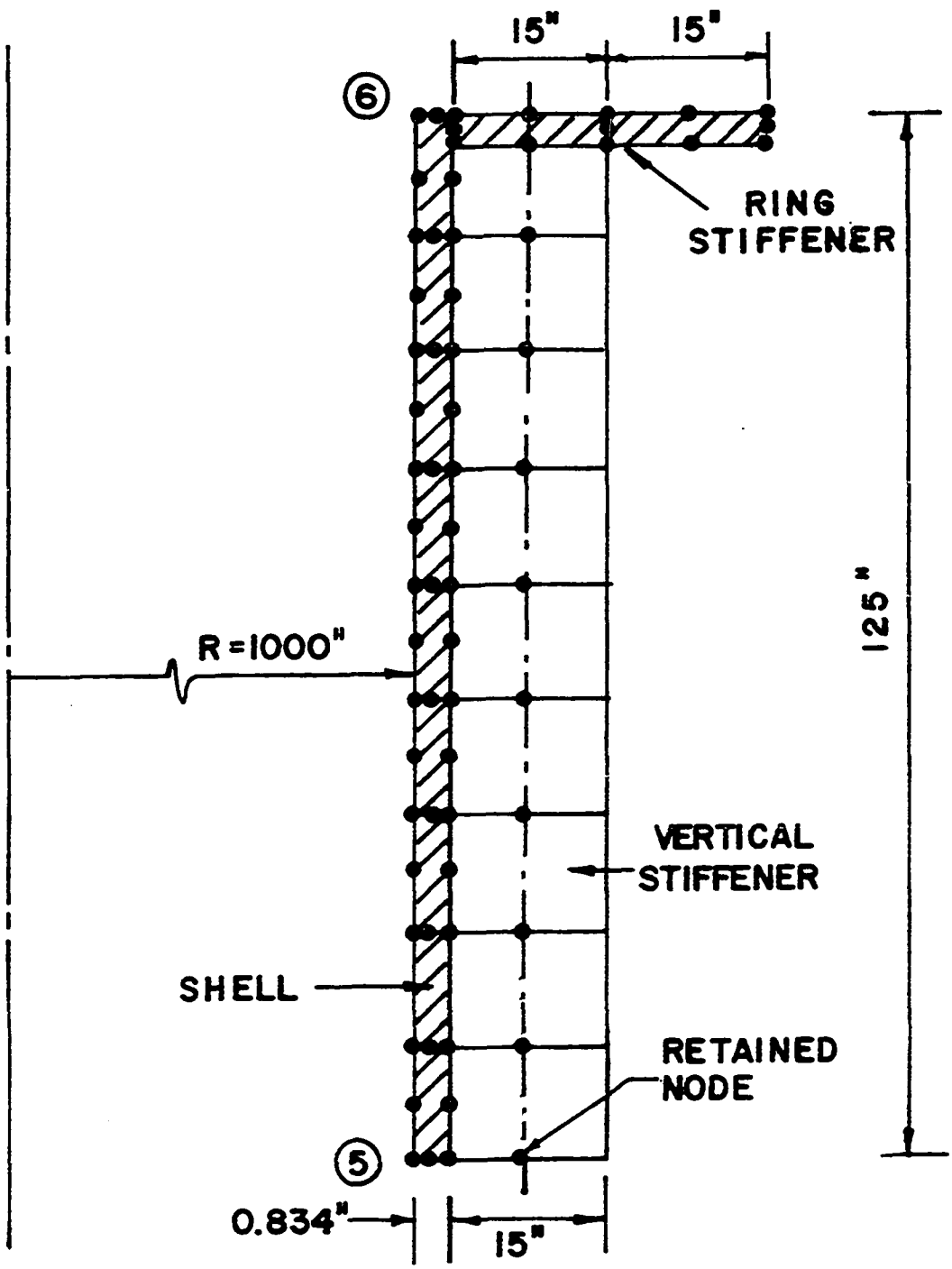

Figure 7. Finite element mesh - axisymmetric idealization

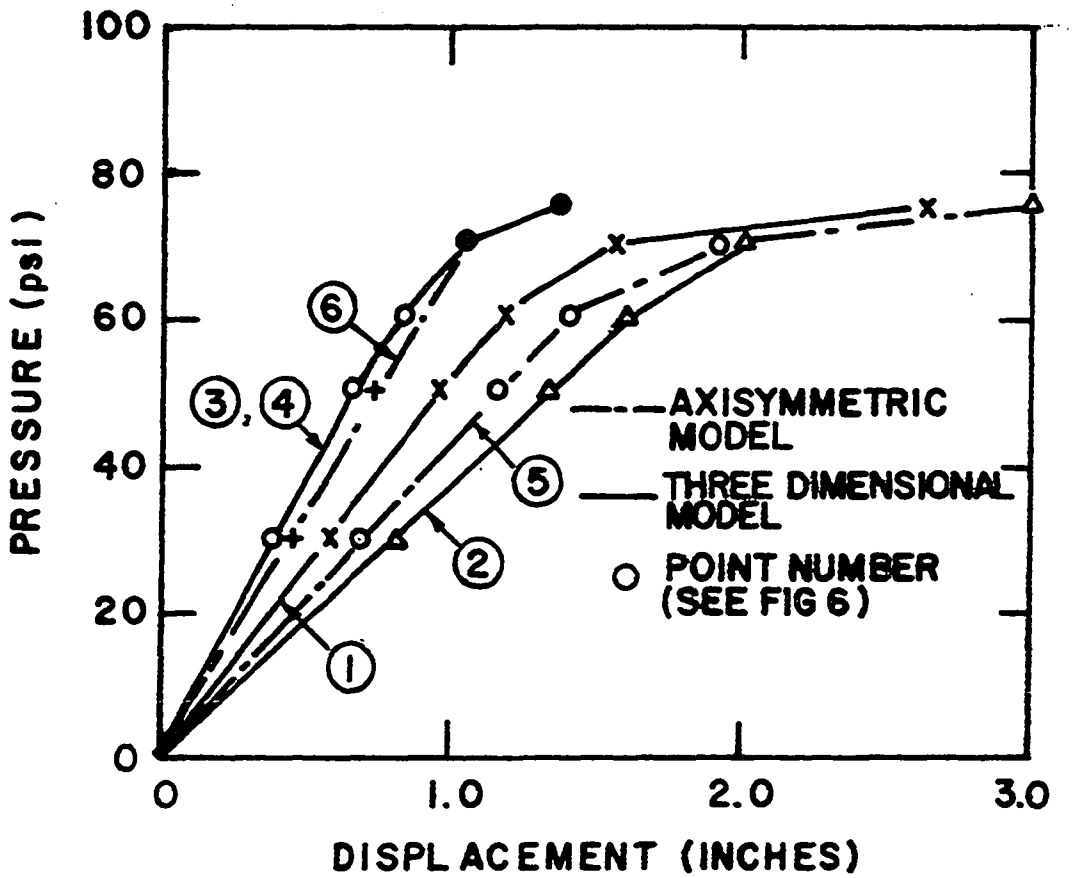

Figure 8. Pressure-displacement curve for a stiffened cylindrical shell panel

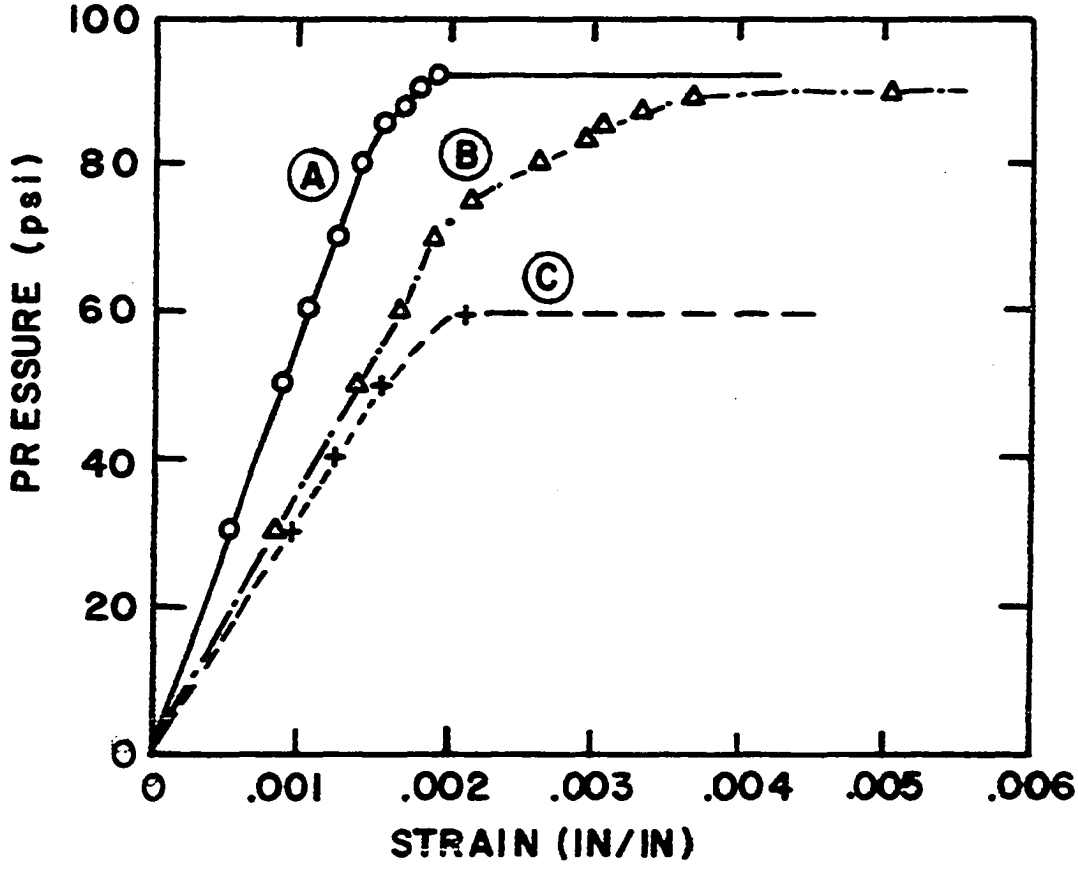

Figure 9. Pressure displacement curves for Models A, B and C, General Failure Mode

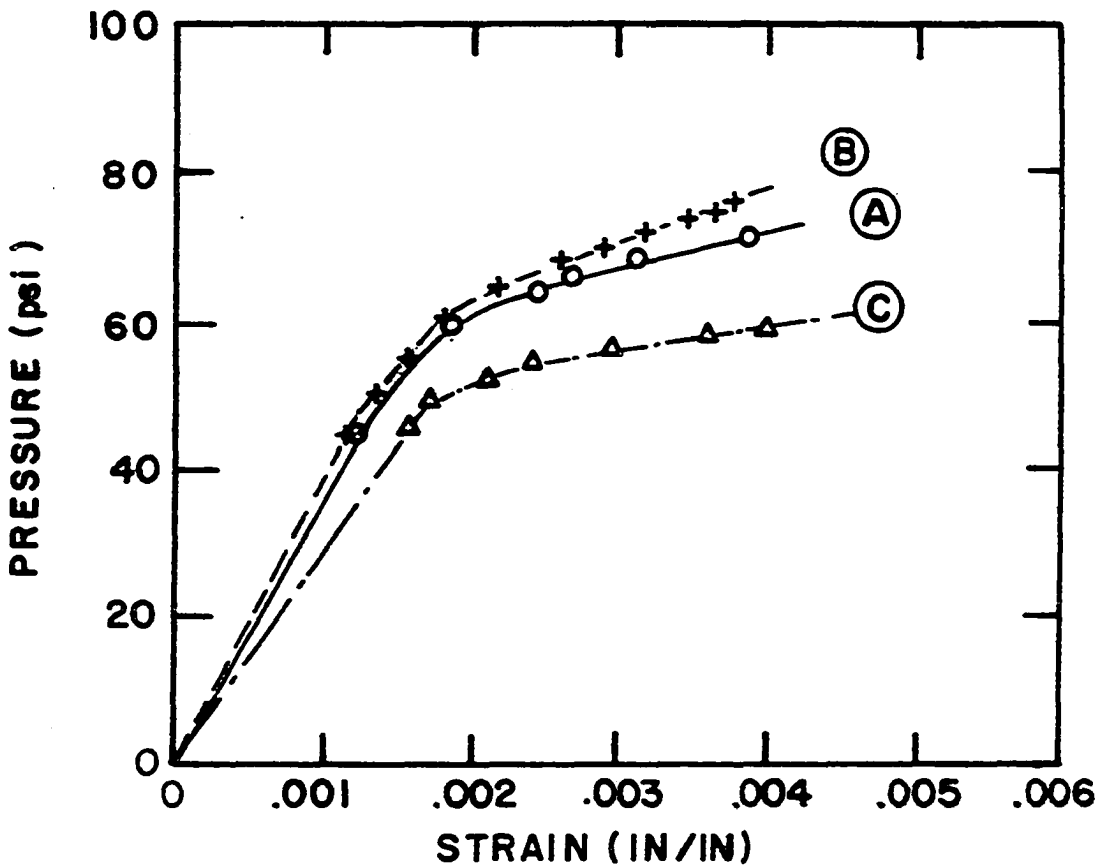

Figure 10. Pressure circumferential strain curves for Models A, B and C, Inter-ring Failure Mode

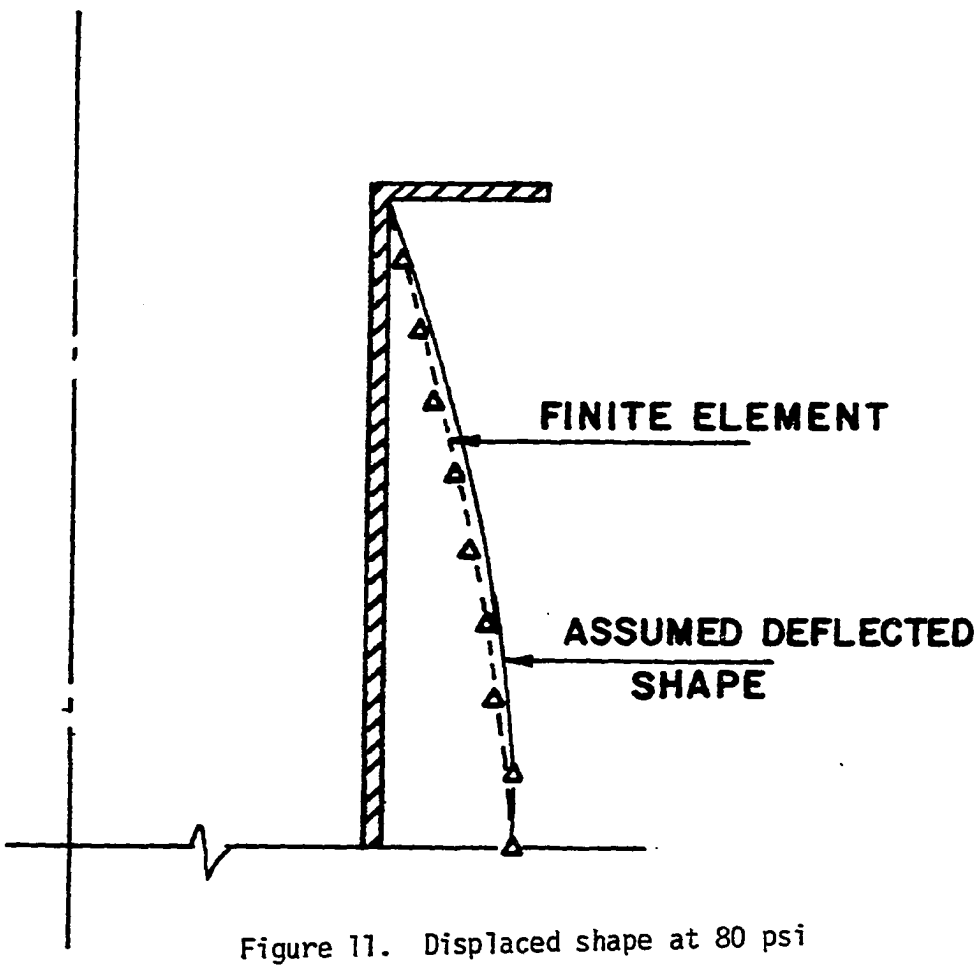

Figure 11. Displaced shape at 80 psi

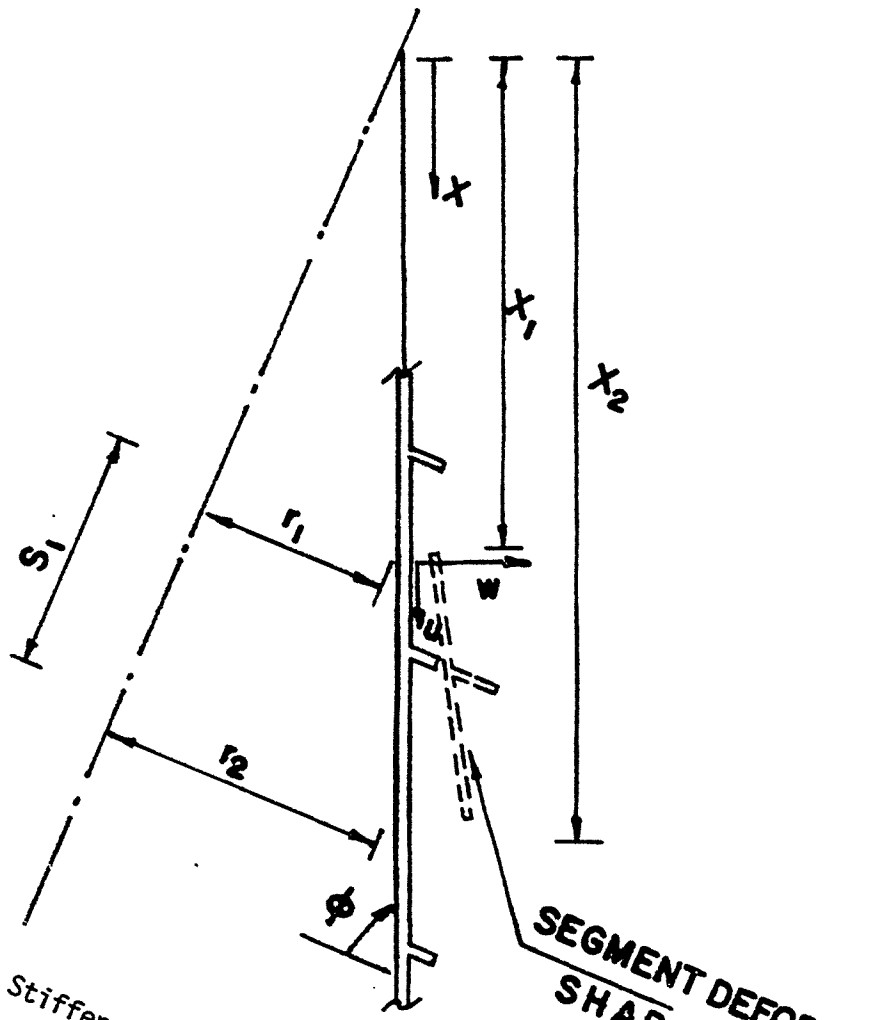

Figure 12. Stiffened conical shell segment, General Failure Mode

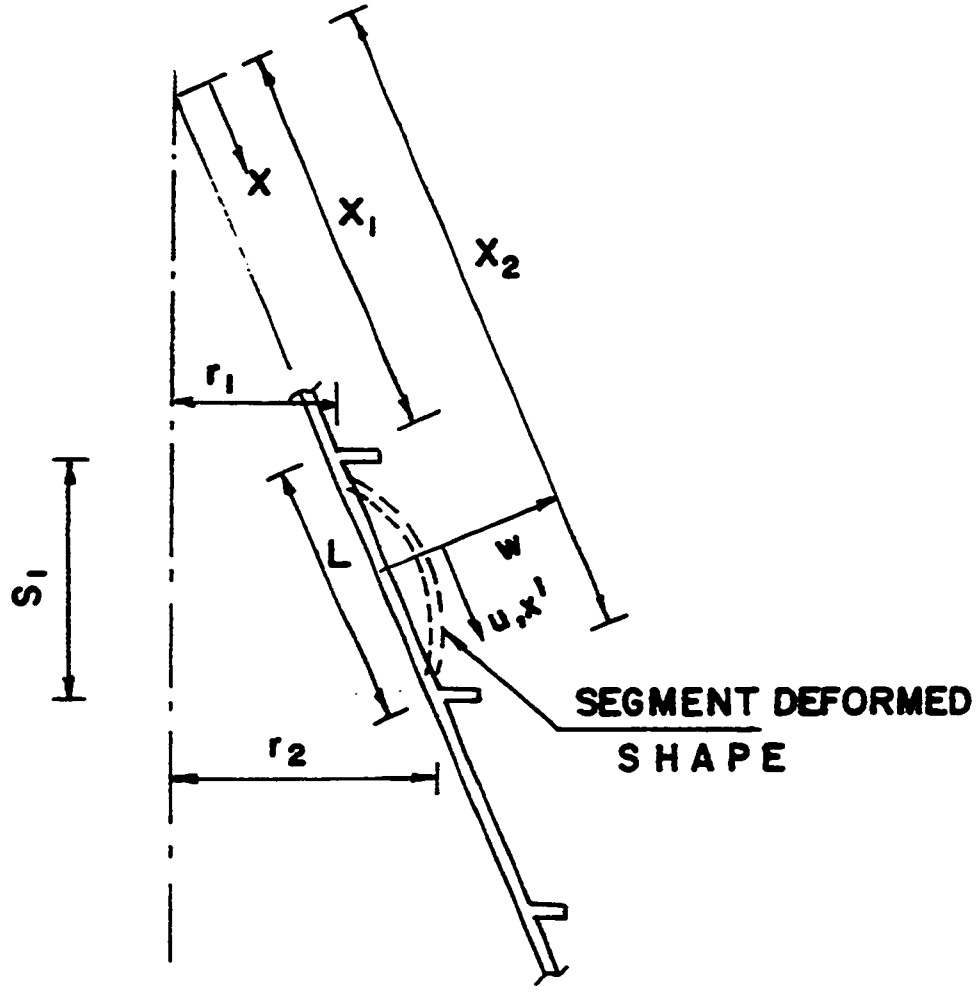

Figure 13. Stiffened conical shell segment, Inter-ring Failure Mode

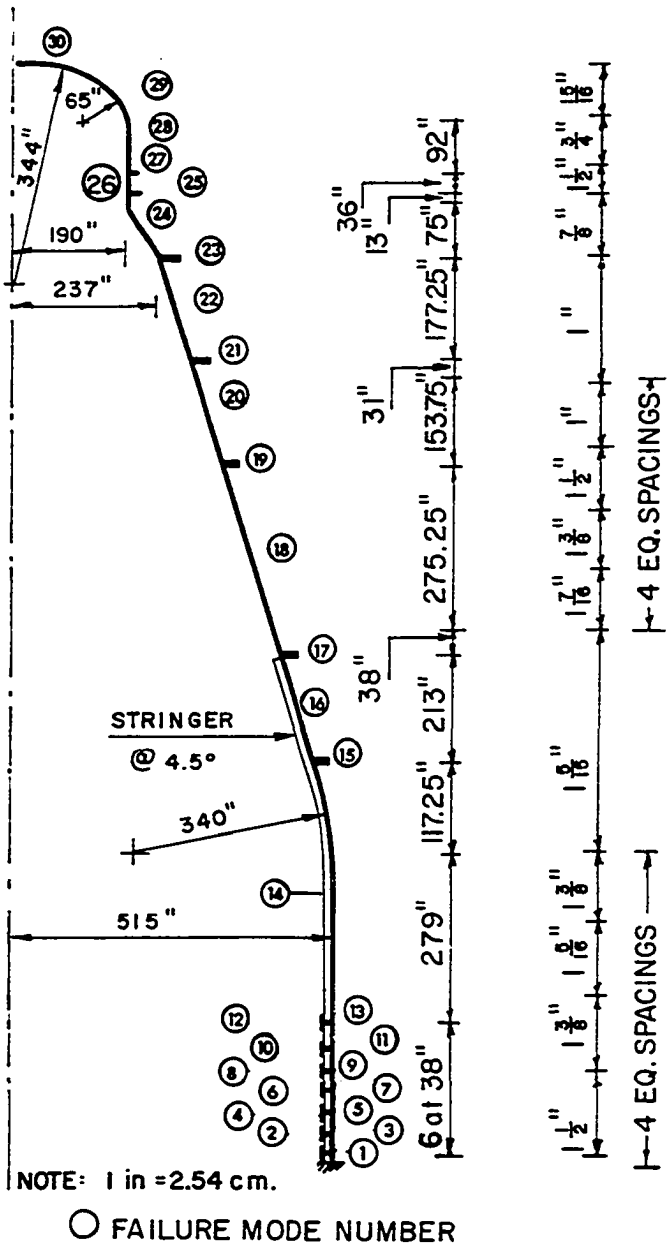

Figure 14. Containment vessel geometry

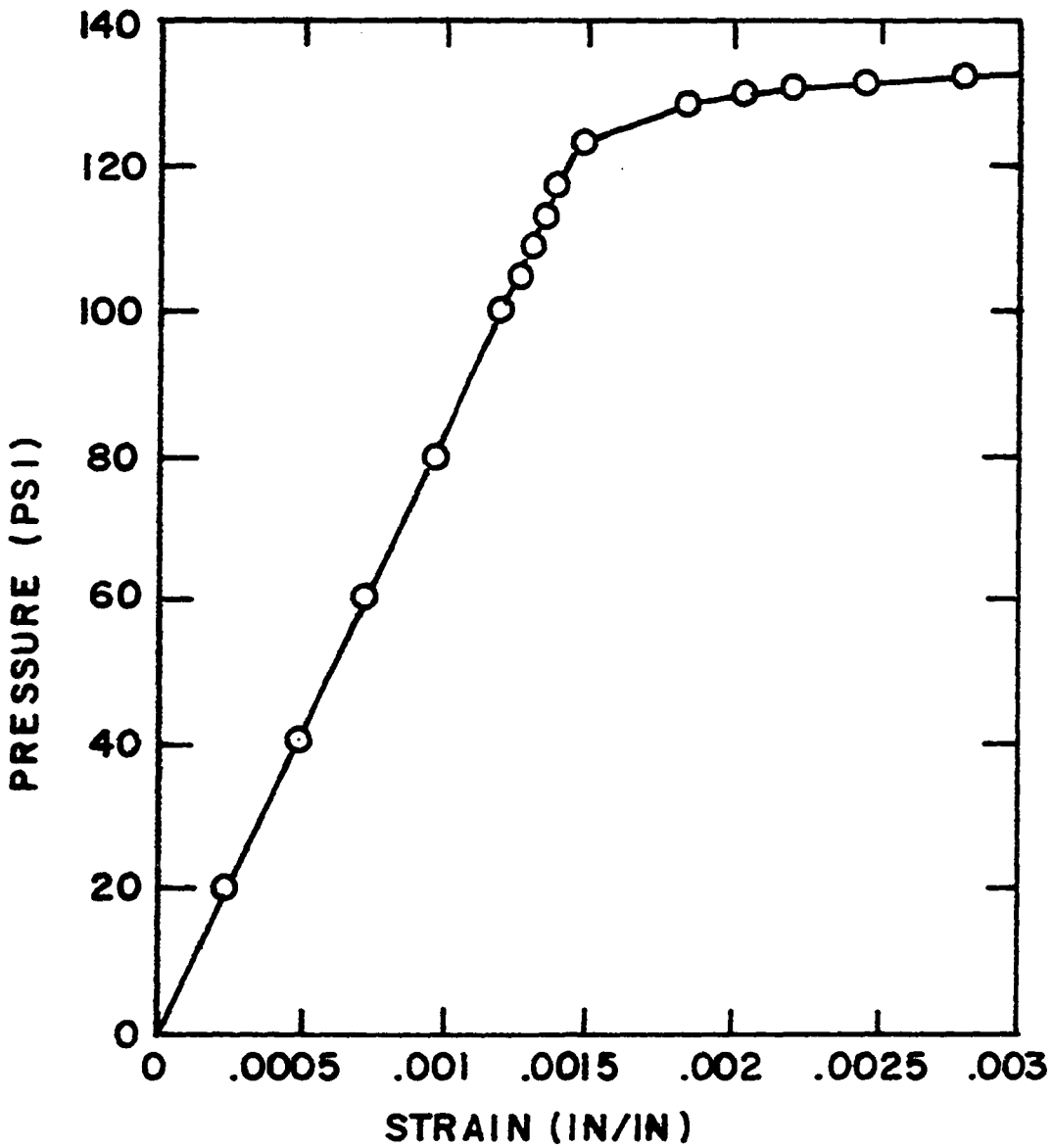

Figure 15. Maximum circumferential membrane strain versus pressure

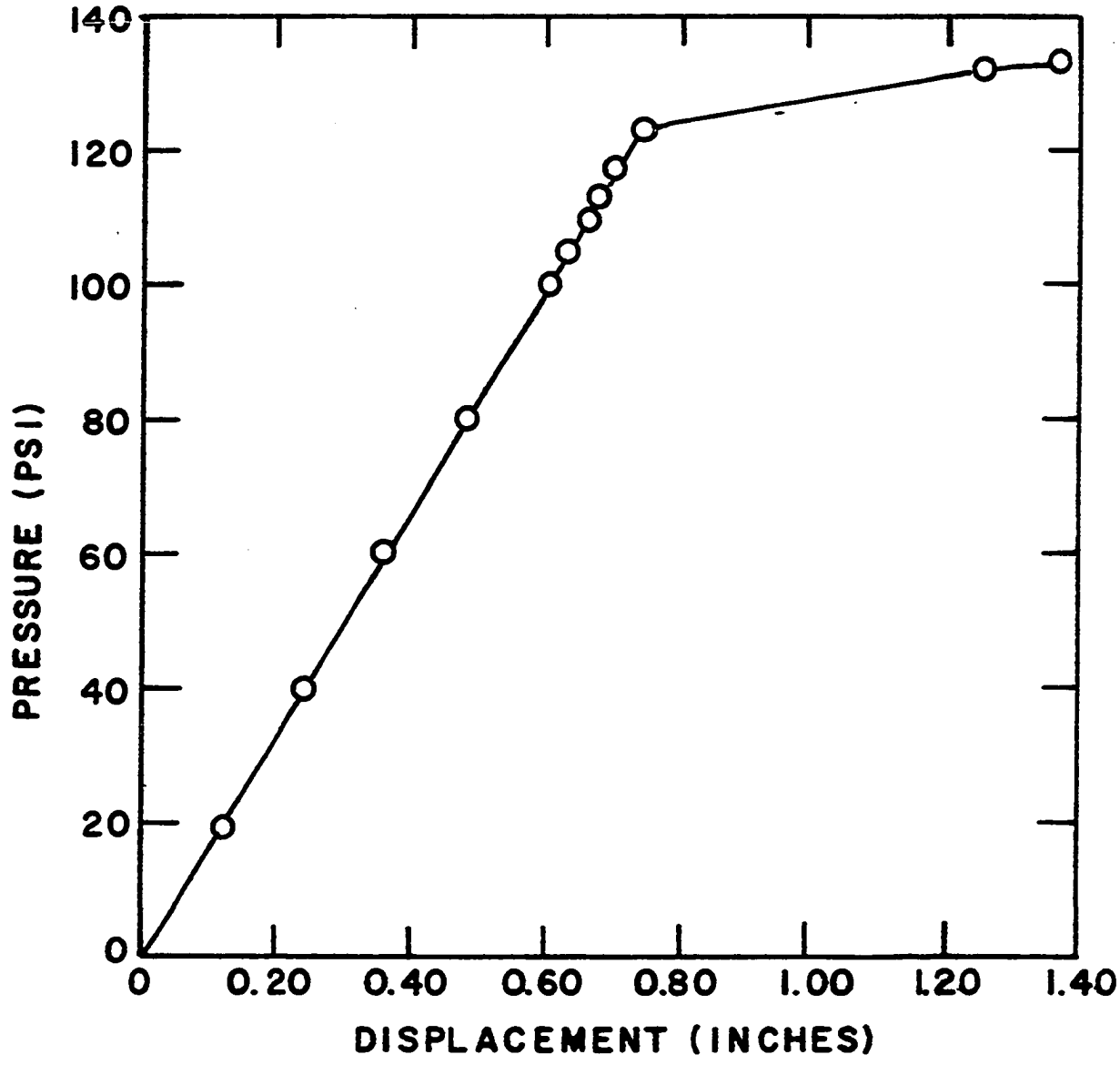

Figure 16. Maximum radial displacement versus pressure

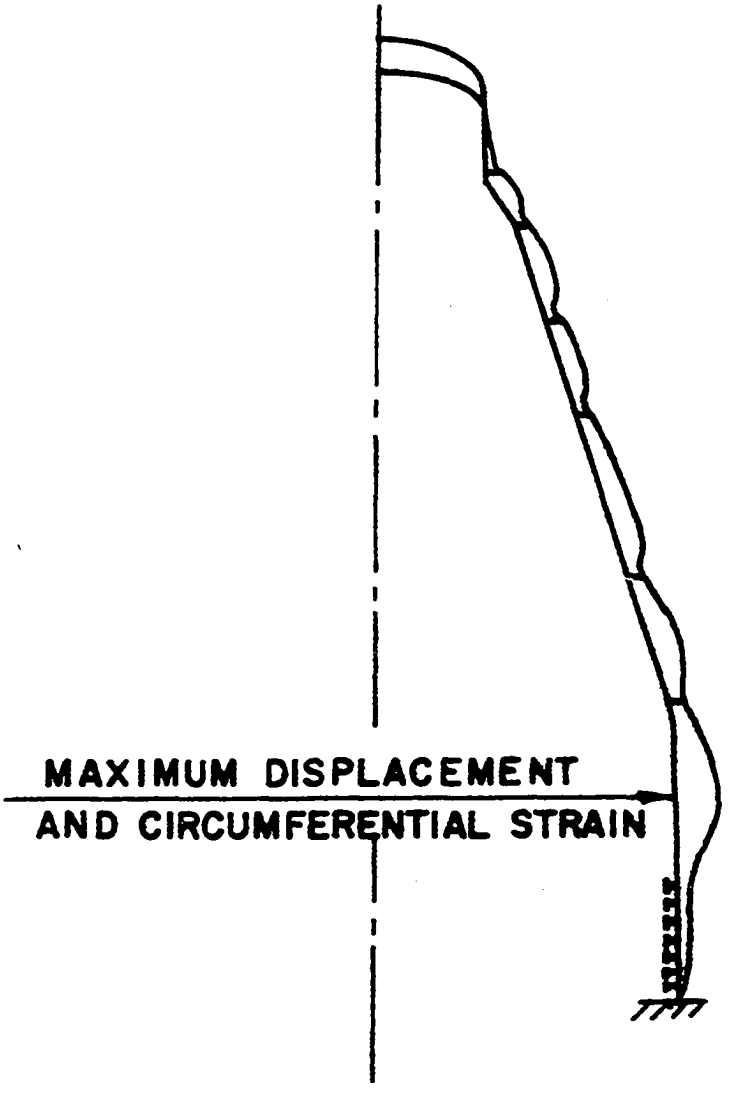

Figure 17. Deformed shape of the containment vessel

PART II. SIMPLIFIED DYNAMIC ANALYSIS FOR INTERNAL LOCALLY LOADED SHELLS

Abstract

The response of axisymmetric shells to localized impulsive loadings that produce large deformations and material nonlinearities is analyzed. Simplified methods for the prediction of the strain ductility of these shells are presented. The methods are developed by idealizing the structure as a single degree of freedom model. Large deformation effects are included and an elastic-perfectly plastic material model is used. Several impulsive problems are analyzed using a finite element technique and the simplified solution. The agreement between the two results indicates that the simplified methods provide an accurate solution at a fraction of the cost of the finite element solution.

Introduction

The calculation of the nonlinear dynamic response of shell structures has received considerable attention in recent years. Most of the literature that has appeared on this subject has concentrated on the snap-through problem. The dynamic response of spherical caps subjected to external loads that cause plastic deformations was conducted using finite element methods (1,2,3,4,5). Finite difference methods (6,7) and finite element techniques (8,9) were used to investigate the dynamic buckling of cylindrical shells. The response of plates, rings, beams and shells under local loads, uniform high intensity impulse

loading and/or blast loading was also studied (10,11,12,13). Closed form analytical solutions for simple beams and circular rings were obtained by Symonds (14) and Duffey and Krieg (15), respectively. In addition, the response of structures in cases involving wave propagation effects has been investigated (16).

In many of the above investigations, numerical integration procedures in conjunction with finite element analysis were used. The problem that consistently arose was the choice of a suitable time step size to perform the time integration. In order to insure stability of the numerical integration and to predict the system dynamic response, the time step size has to be sufficiently small (17,18). This is particularly true when the structure is subjected to short duration loads in which a large number of high modes are excited or in cases involving wave propagation modes. These small time step computations are very expensive. An alternative is to adopt simplified methods which permit rapid analysis of even complex structures, with reasonable accuracy.

The following work represents a portion of a total program whose objective is to assess the uncertainty of the containment vessel resistance. One part was devoted to developing simplified methods to analyze stiffened axisymmetric shells under uniform internal static pressure. The present part, discussed herein, concentrates on the dynamic analysis of unstiffened axisymmetric structures subjected to internal localized dynamic loads. Simplified approaches for the prediction of the maximum deformation of cylindrical and spherical shells under high intensity localized loading are proposed. These methods are based upon

idealizing the structure and the applied loads to simulate an elastic-plastic single degree of freedom model. Additionally, the methods take into account large deformations effects. The one degree of freedom system is traditionally expedient for obtaining the response of structures in the plastic range (19). Finite element analyses are used to guide the formulation and to calibrate the simplified methods.

Simplified Dynamic Analysis of Axisymmetric Shells

General

The problem of evaluating the resistance of axisymmetric shells under localized dynamic load is an important one, for example, containment vessels for nuclear power plants. Localized dynamic loads could possibly be generated within the containment shell by hydrogen explosions. A hydrogen detonation within the confines of the containment generates a shock wave which propagates through the air inside the containment. When this shock wave intersects the containment walls, a reflected pressure is generated which delivers dynamic pressures to the shell. Such a type of loading can be idealized as a pure impulse. This is very close to true if the pulse length of the dynamic pressure is less than one-fifth the predominant structural period (19). In the following discussion, simplified methods for the evaluation of the maximum deformation of an impulsively loaded cylindrical and spherical shells are presented. These methods are based upon using the Rayleigh-Ritz approach with an assumed displaced shape (19,20). Finite element analyses will be employed to guide the formulation.

Simplified dynamic analysis of cylindrical shells

For an axisymmetric structure with nonsymmetric applied loads (see Fig. 1), the membrane strain displacement relationships which include large rotation effects are (21):

$$\varepsilon_{\phi} = \frac{du}{dx} + \frac{1}{2}\left(\frac{dw}{dx}\right)^2 \tag{1}$$

$$\varepsilon_{\theta} = \frac{dv}{dy} + \frac{w}{r} + \frac{1}{2}\left(\frac{dw}{dy}\right)^2 \tag{2}$$

$$\gamma_{\theta\phi} = \frac{dv}{dx} + \frac{du}{dy} + \frac{dw}{dx}\frac{dw}{dy} \tag{3}$$

in which ε_{ϕ}, ε_{θ} and $\gamma_{\theta\phi}$ are the meridional, circumferential and shear strain, respectively. The displacements w, u and v, , are the radial, meridional and circumferential displacements, respectively. x and y are the cylinder meridional and circumferential coordinates, respectively, while r denotes the shell midsurface radius.

Figure 1 illustrates a deformed shape for a smooth cylindrical shell subjected to a localized load. The dynamic load is idealized as an impulsive pressure applied over a circular area, with a radius s_o. The displaced shape is assumed to vary as an elliptic paraboloid with major and minor radii of a and b, respectively (see Fig. 1). This shape is close to actual when the deformations of the shell are significantly into the plastic stage. This assumption will be approximately

verified later in this study. For the above assumed shape, the radial displacement w is written as:

$$w = w_o \left(1 - \frac{x^2}{a^2} - \frac{y^2}{b^2}\right) \tag{4}$$

in which w_o represents the maximum displacement normal to the shell surface at the ellipse centroid. The associated circumferential and meridional membrane strains are also assumed to vary with the same shape and are written as:

$$\varepsilon_\theta = \varepsilon_{\theta_o} \left(1 - \frac{x^2}{a^2} - \frac{y^2}{b^2}\right) \tag{5}$$

$$\varepsilon_\phi = \varepsilon_{\phi_o} \left(1 - \frac{x^2}{a^2} - \frac{y^2}{b^2}\right) \tag{6}$$

where $\varepsilon_{\theta o}$ and $\varepsilon_{\phi o}$ are the maximum strains at the centroid of the deformed area (see Fig. 1). In this study, the strain energy associated with the shear strain is neglected compared to the strain energy due to the circumferential and meridional strains.

As previously mentioned, the dynamic analysis will be accomplished using an equivalent, elastic-plastic single degree of freedom system. In order to define an equivalent one degree of freedom model, it is

necessary to evaluate the parameters of such a system, namely, the equivalent mass m^*, stiffness k^*, maximum spring force R_m^*, and the equivalent force F^*. With this representation of the actual structure, the dynamic analysis becomes relatively simple. By equating the kinetic and potential energy of the actual and equivalent model in conjunction with the assumed shape given in Eq. 4, one obtains, for example, the equivalent force, F^*, which is expressed as (19):

$$F^* = \int_{A_0} p\, w\, dA \tag{7}$$

when A_0 is the area over which the pressure p is applied. Integration of Eq. 7 yields:

$$F^* = \pi s_0^2\, p \left[1 - \frac{s_0^2}{4}\left(\frac{1}{a^2} + \frac{1}{b^2}\right)\right] \tag{8}$$

In the case of an applied impulse, i, per unit area, the equivalent impulse I^* for the idealized single degree of freedom model can be written as:

$$I^* = \pi s_0^2\, i \left[1 - \frac{s_0^2}{4}\left(\frac{1}{a^2} + \frac{1}{b^2}\right)\right] \tag{9}$$

In a similar way, the equivalent mass, m^*, is calculated using the following relation (19):

$$m^* = \int_{A_d} m\left(1 - \frac{x^2}{a^2} - \frac{y^2}{b^2}\right)^2 dA \tag{10}$$

in which A_d represents the area of the assumed deformed shape on which the equivalent system is based. Integration of Eq. 10 results in:

$$m^* = \frac{\pi m a b}{3} \tag{11}$$

where m is the mass of the shell skin per unit area. By impulse momentum principles, the initial velocity, $\dot{w}_o$, of the equivalent system can also be written as:

$$\dot{w}_o = \frac{I^*}{m^*} \tag{12}$$

Initially, when an explosion occurs inside a containment, an impulse is delivered to the undisturbed vessel walls. In other words, the energy is all in the form of kinetic energy, T, and can be expressed for the equivalent single degree of freedom model as:

$$T = \frac{1}{2} m^* \dot{w}_o^2 \tag{13}$$

Substituting Eqs. 9 and 11 into the above relationship yields:

$$T = \frac{3\pi s_o^4 i^2}{2 a b m} \left[1 - \frac{s_o^2}{4} \left(\frac{1}{a^2} + \frac{1}{b^2}\right)\right] \tag{14}$$

At the maximum displacement, i.e., zero velocity, the kinetic energy has been changed to strain energy. This energy is given as:

$$U = \int_v (f_\theta \varepsilon_\theta + f_\phi \varepsilon_\phi) \, d v \tag{15}$$

in which f_θ and f_ϕ, are the circumferential and meridional membrane stresses, respectively. In Eq. 15, bending energy is neglected since, for large displacements, the behavior is principally membrane, as the finite element analyses demonstrate. The von Mises yield criterion (22) is employed in this investigation to relate the membrane stresses to the material yield strength, F_y, as:

$$f_\theta^2 + f_\phi^2 - f_\theta f_\phi = F_y^2 \tag{16}$$

The plastic strains ε_θ and ε_ϕ for a rigid-perfectly plastic material, according to the deformation strain theory of plasticity (22), are as follows:

$$\varepsilon_\theta = C\,(f_\theta - \tfrac{1}{2} f_\phi) \tag{17}$$

$$\varepsilon_\phi = C\,(f_\phi - \tfrac{1}{2} f_\theta) \tag{18}$$

in which C denotes a proportionality constant. The maximum membrane strains, ε_{θ_0} and ε_{ϕ_0}, are also assumed to be related to each other as:

$$\frac{\varepsilon_{\theta_0}}{\varepsilon_{\phi_0}} = \frac{a}{b} \tag{19}$$

Introducing Eq. 19 into Eqs. 17 and 18 yields the following relationship between the membrane stresses f_θ and f_ϕ

$$f_\phi = \left(\frac{2b + a}{2a + b}\right) f_\theta \tag{20}$$

Substituting the above relationships into Eq. 15 results in the following strain energy accumulation for a rigid-perfectly plastic material:

$$U = \frac{\pi\, b\, t\, F_y\, \varepsilon_{\theta_0}}{\sqrt{3}} \left(a^2 + b^2 + ab\right)^{1/2} \tag{21}$$

in which t is the thickness of the shell wall.

The strain energy given in Eq. 21 can be modified to approximate the case of an elastic-perfectly plastic material. Since the stress-strain relationship is linear in the elastic region, the strain energy, U_e, which is accumulated up to the yield strain, ε_y, can be approximated as:

$$U_e \simeq \frac{1}{2} U \Big|_{\varepsilon_{\theta_o} = \varepsilon_y} \tag{22}$$

in which U is the energy associated with rigid-perfectly plastic behavior. Subtracting this complementary elastic energy from the energy given by Eq. 21, the internal energy for an elastic-perfectly plastic material can be approximated as:

$$U = \frac{\pi\, bt\, F_y}{\sqrt{3}} (a^2 + b^2 + ab)^{1/2} (\varepsilon_{\theta_o} - \frac{1}{2} \varepsilon_y) \tag{23}$$

Eq. 23 can be written in terms of a strain ductility, λ, as:

$$U = \frac{\pi\, bt\, F_y\, \varepsilon_y}{\sqrt{3}} (a^2 + b^2 + ab)^{1/2} (\lambda - \frac{1}{2}) \tag{24}$$

where

$$\lambda = \frac{\varepsilon_{\theta_o}}{\varepsilon_y} \tag{25}$$

During the dynamic response of the shell, the initial kinetic energy (Eq. 14) is converted into internal strain energy as the single degree of freedom system reaches a maximum displacement (zero velocity). Equating Eqs. 14 and 24, one obtains:

$$i^2 = \psi \frac{2m\, t\, F_y\, \varepsilon_y}{3\sqrt{3}} (\lambda - \tfrac{1}{2}) \tag{26}$$

where

$$\psi = \frac{A\, B^2\, (A^2 + B^2 + AB)}{\left[1 - \frac{1}{4}\left(\frac{1}{A^2} + \frac{1}{B^2}\right)\right]^2}^{1/2} \tag{27}$$

in which

$$A = \frac{a}{s_o} \tag{28}$$

$$B = \frac{b}{s_o} \tag{29}$$

To this point, the constants a and b, which define the assumed dis-

placed shape have not been identified, i.e., the extent of the deformation has not been selected. These parameters will be selected to minimize the collapse load (impulse) (23):

$$\frac{\partial i}{\partial A} = 0 , \quad \frac{\partial i}{\partial B} = 0 \tag{30}$$

This analytical procedure results in coupled equations from which the unknown parameters A and B can be calculated. For an impulsively loaded cylindrical shell, the parameters A and B are found to satisfy Eq. 30 when both are unity:

$$A = B = 1 \tag{31}$$

or

$$a = b = s_0 \tag{32}$$

In other words, the boundary of the assumed deformed shape coincides with the boundary of the applied load. This will be verified by finite element analysis in the following sections. Substituting the relationship given in Eq. 31 into Eq. 26 produces:

$$\lambda = \frac{3\, i^2}{8\, m\, t\, F_y\, \varepsilon_y} + \frac{1}{2} \tag{33}$$

in which λ can be interpreted as the ductility demand associated with the impulsive pressure i. In summary, Eqs. 26 and 33 represent the approximate dynamic solution of the problem shown in Fig. 1 with a prescribed impulsive load.

Simplified dynamic analysis of spherical shells

The preceding method can be specialized to analyze locally loaded spherical shell structures. In this case, the impulse delivered to the shell walls produces symmetric deformations in the shell skin. This is an axisymmetric problem, and, hence, the assumed shapes in Eqs. 4, 5 and 6 become:

$$w = w_o \left[1 - \left(\frac{x}{a}\right)^2\right] \tag{34}$$

$$\varepsilon_\theta = \varepsilon_{\theta_o} \left[1 - \left(\frac{x}{a}\right)^2\right] \tag{35}$$

$$\varepsilon_\theta = \dot{\varepsilon}_\phi \tag{36}$$

Following the procedure outlined in the foregoing section yields:

$$\psi = \left[\frac{A^2}{1 - \frac{2}{A^2}}\right]^2 \tag{37}$$

Applying the minimization procedure given by Eq. 30 results in the following relationships for a localized loaded spherical shell:

$$i^2 = \frac{8\, m t F_y \varepsilon_y}{3} (\lambda - \frac{1}{2}) \tag{38}$$

$$\lambda = \frac{3\, i^2}{8\, m\, t F_y \varepsilon_y} + \frac{1}{2} \tag{39}$$

As can be seen, Eq. 39 is identical to Eq. 33. The strain ductility in a cylindrical or spherical shell due to short duration impulse loading is independent of the shell radius r. In other words, one can conclude that there is no difference in the strain ductility demand of a cylindrical or spherical shell having the same wall thickness, t, and subjected to the same impulse, i. Additionally, the strain ductility of a circular plate could be predicted using the above relations since Eqs. 33 and 39 demonstrate that the strain ductility is independent of the shell radius of curvature. This finding will be approximately verified by finite element analyses in the following sections.

Calibration of the Simplified Methods

Several assumptions were involved in the formulation and the development of the simplified methods. Verification and calibration of these approaches will be conducted by comparing the results with finite element results. The ANSYS (24) finite element computer code was used in this work to perform the transient nonlinear dynamic analysis of

locally loaded shells.

Finite element guidelines

The ANSYS program is a large-scale, general-purpose finite element program for the solution of several classes of engineering analysis problems. Geometric nonlinearity can be included by either one or both of two possible options in the program. The first option is called stress stiffening and is accomplished by adding the geometric stiffness matrix (25) to the usual linear element stiffness matrix. The second, referred to as large displacement analysis, is accomplished by updating nodal coordinates to formulate the element stiffness matrix (25). Reference 26 recommends using both the stress stiffening and large displacement options for flexible structures with low bending stiffness. The ANSYS program also provides several options which can be used to solve for material nonlinearity effects. An elastic-perfectly plastic material property is employed in this work.

In performing the nonlinear transient dynamic solution of impulsively loaded shells, it is expedient to start with the simple case, i.e., a spherical shell. A uniform impulse is applied to the sphere over a local area as shown in Fig. 2. In this work, the angle, β_0 (see Fig. 2), of the loaded area is taken a 3.3 degrees. In addition, only a portion of the sphere is used for the finite element analysis, since the influence of the displacement boundary conditions does not propagate out beyond an angle of five times $\sqrt{t/r}$ (27). The author recognizes that this may not be true if the impulsively loaded

structure behaves elastically (because of wave propagation and reflection effects). However, the deformed shape becomes very localized when the structural behavior is predominantly nonlinear. This approximation will be verified later.

As part of the study presented herein, the following effects on the finite element dynamic results were investigated. First of all, the effect of the finite element model, in particular, the arc length used to model the spherical shell, was studied. Second, the influence of the impulse shape was examined. Also, the effect of the integration time step size was investigated. These studies were conducted using a spherical shell with a radius of 1000 in. (25.4 m), an r/t ratio of 2400, and a material yield strength of 50 ksi (344.5 MN/m^2). The sphere was subjected to an initial impulse equivalent to an initial velocity condition of 2000 in/sec (50.8 m/sec) within the localized angle β_0 (see Fig. 2). A portion of the sphere with an angle, ϕ_0 (see Fig. 2), of fifteen degrees was used for the finite element model. This was idealized for the finite element analysis by a number of three-dimensional triangular shell elements. The element has both bending and membrane capabilities and six degrees of freedom at each node. (This element is referred to as STIF 48 in the ANSYS element library.) The element length was restricted to $\sqrt{rt}/2$ within and near the loaded area but was gradually increased toward the outer edge; however, the element aspect ratio was kept less than two. A five-degree wedge of the spherical cap was analyzed because of the circular symmetry (see Fig. 2). The conditions of symmetry were imposed at

each of the boundaries. Complete details of the above studies are given in the Appendix.

The study verified that a spherical cap with an angle ϕ_0 of fifteen degrees is adequate for the finite element idealization of the spherical shell since the results did not differ significantly when a 30 degree cap was analyzed. A uniformly distributed pure impulse was found to approximate adequately the pressure-time loading. Finally, the procedure suggested in Ref. (16) will be adopted to account for the effects of the time step size on the numerical integration results. In this procedure, the problem is solved a number of times with different time step sizes and the "best" answer selected (16). In the current work, each problem is analyzed at least twice and the results are linearly extrapolated to a zero time step size. The author recognizes that this approach may underestimate the final strain results.

Analysis of spherical shells

As a part of the calibration of the simplified methods presented, the following spherical shells were analyzed. Two spheres with a radius of 1000 in. (25.4 m) and an r/t ratio of 2400 (Sphere I) and 1200 (Sphere II), respectively, were considered. A uniform pure impulse (initial velocity) was applied within an area with angle β_0 of 3.3 degrees. Sphere I was analyzed with initial velocities of 2000 in/sec (50.8 m/sec) and 1000 in/sec (25.4 m/sec). The solution of Sphere II was conducted using an initial velocity of 2000 in/sec (50.8 in/sec). The analysis of both problems was carried out until the first zero

velocity peak of the structure response (maximum circumferential membrane strain) was reached.

Some of the finite element results for Sphere II with a time step size of 50 μsec are summarized in Figs. 3, 4, 5, 6, 7 and 8. Figures 3 and 4 illustrate the circumferential membrane strain and the crown radial displacement, respectively, as functions of time. Figure 5 shows the normalized circumferential membrane strains (strain/maximum strain). The normalized radial displacements (nodal displacement/crown radial displacement) versus the arc length measured from the crown are shown in Fig. 6. The assumed parabolic deformed shape given by Eq. 34 is also illustrated. Notice that the effect of the localized disturbance does not propagate out beyond an angle of three to five times $\sqrt{t/r}$ and certainly not out to fifteen degrees.

Figures 7 and 8 illustrate the maximum circumferential membrane strain and the maximum crown displacement, respectively, as the time step size is reduced for the Sphere I and II solutions. The smaller time step yields higher displacements and strains. As previously mentioned, a good approximation to the solution is predicted by extrapolating these results to zero time step size. These approximate values of the final strain and displacement are given in Table 1. The strain ductilities predicted by the finite element analysis and those calculated using Eq. 39 are also listed. In addition, for the reader's interest, the total computer time (VAX 11/780) used for each solution is tabulated.

The results listed in Table 1 demonstrate that the simplified

analysis predicts a larger strain ductility demand than the finite element method. The finite element analysis would predict higher values if smaller time step sizes were used in extrapolating the results to approximately zero. For example, extrapolating the results of the 50 and 25 μsec time step solutions predicts a ten percent higher strain ductility than the extrapolated 100 and 50 μsec solutions.

Analysis of cylindrical shells

As a continuation of the simplified methods calibration, a locally loaded finite length cylinder was analyzed. The cylinder has a radius of 1000 in. (25.4 m) and an r/t ratio of 1200. A pure uniform impulse that provides an initial velocity of 2000 in/sec (50.8 m/sec) over a localized area with an angle β_0 of 3.3 degrees was considered.

The cylindrical shell was modeled for the finite element analysis using a portion of the cylinder with a one-half central angle of 15 degrees and a length equal to one-half the radius. Once again, the idealization is based upon the finite element guidelines which were discussed previously. The finite element model is shown in Fig. 9. The conditions of symmetry were imposed at each of the boundaries 1-2 and 1-4. The circumferential displacements along the boundary 2-3 were constrained to have the same meridional translation.

The finite element analysis was conducted using time increments of 100 μsec and 50 μsec and the solution was carried out until the first zero velocity peak of the structural response was reached. The extrapolation procedure discussed previously was used to predict the maximum

circumferential membrane strain and outward displacement. These results are summarized in Table 1. The normalized radial displacements of the nodes along boundary 1-2 (nodal point displacement/maximum displacement) are plotted in Fig. 6. The normalized circumferential membrane strains of the elements along the boundary 1-2 are superimposed on Fig. 5. Figure 10 illustrates the deformed shape of the locally loaded cylindrical shell. Notice that the radial displacements decay rapidly toward the boundary of the loaded area. Also, notice that the boundary of the deformed shape forms a circle which coincides closely with the loaded area boundary. These findings confirm the assumptions stated early in this work.

Analysis of circular plates

In order to extend the applicability of the simplified methods discussed previously, a nonlinear dynamic analysis of a circular plate was performed. The plate had a radius of 260 in. (6.60 m) and a 0.8333 in. (2.117 cm.) thickness. These dimensions were employed to resemble the spherical cap analyzed previously (Sphere II). The plate was subjected to pure uniform impulse which amounts to an initial velocity of 2000 in/sec. (50.8 m/sec.) over a circular area of a radius equal to 57.5 in. (1.461 m). This is equivalent to the loaded area used in the spherical and cylindrical shell study. The finite element solution was conducted using time step sizes of 100, 50 and 25 μsec. up to the first strain peak reached. A summary of the finite element results is shown in Figs. 3, 4, 5 and 6 where they are superimposed on the corresponding

results for the cylinder and sphere analysis. The maximum normal deflection and maximum strain were predicted using the extrapolation procedure mentioned before and are given in Table 1. The strain ductility predicted using Eq. 39 is also shown.

General discussion

The analyses described in the previous sections were performed in order to verify the proposed simplified methods. Table 1 summarizes the finite element analysis of the different structures analyzed. As can be seen, the finite element analysis results in a smaller strain ductility than the simplified methods. However, larger finite element results would be predicted if very small time step sizes were employed in the analysis. Additionally, a larger value of the maximum strain could possibly be reached at some later response peak since the finite element solutions presented were carried out only to the first peak. While this is possible, it would be very expensive in terms of computer time (see the listed computer time in Table 1). On the other hand, one can see the advantages of using the simplified methods presented in this work. This approach predicts higher strain ductilities, which are probably closer to the correct answer.

The finite element results for the sphere, cylinder and plate are interestingly similar. Each structure behaves differently in the early stage, i.e., in the elastic region, as would be predicted by linear shell theory. When the deformations become large; however, (see Fig.

6) the strains are found to have little variation through the thickness, i.e., the bending strains are insignificant and the membrane effects predominate. Additionally, even though the sphere, cylinder and plate initially have dissimilar radii of curvature, these differences are insignificant when compared to the highly localized curvature and shape associated with the large displacement. The simplified result of Eqs. 33 and 39 also predict this when one notices that the ductility is independent of the radius of curvature in both the cylindrical and spherical solutions. Figures 5 and 6 illustrate the similarities in the strains and displacements for the sphere, cylinder and plates as well as a comparison with the assumed functions.

Conclusions

The nonlinear transient dynamic of an impulsively loaded shell is, in general, expensive. Alternative approaches referred to as simplified methods are developed. These methods are based upon idealizing the structure as an elastic-plastic single degree of freedom model with large deformation effects. Finite element techniques were used to guide and calibrate the formulation of these methods. Three different shells were analyzed using the finite element technique and simplified approach. The simplified methods are sufficiently accurate to define the strain ductility of an impulsively loaded cylindrical shell, spherical shell and circular plates. These methods demonstrate that the

ductility is independent of the radius of curvature which is confirmed by the finite element analysis. The methods represent a powerful tool for practical applications. On the other hand, the finite element provides an accurate solution only at large expense -- small time steps.

Appendix. Finite Element Modeling Guidelines

The objective of the study summarized in the Appendix is to investigate the influence of the following parameters on the finite element dynamic analysis:

1. Finite element model.
2. Impulse shape.
3. Time step size.

To study these three different effects, a nonlinear transient analysis of the spherical shell shown in Fig. 2 was performed. The shell radius and thickness are 1000 in. (25.4 m) and 0.417 in. (1.06 cm.), respectively. A pure impulse per unit area of 0.617 psi-sec. was applied to the shell crown as shown in Fig. 2. This impulse was taken to be uniformly distributed over a localized circular area with an angle, β_0, of 3.3 degrees (see Fig. 2). Such an impulse amounts to a specified initial velocity condition of 2000 in/sec. (50.8 m/sec.). The material yield strength and Young's modulus were taken a 50 ksi (345 MN/m^2) and 30,000 ksi (207,000 MN/m^2), respectively.

The finite element solution was conducted using the ANSYS finite element computer program. The analysis was accomplished taking into account geometric and material nonlinearity effects. The large displacement and stress stiffening options available in the program were employed. An elastic-perfectly plastic material was used.

To investigate the effect of the finite element, a solution of the problem shown in Fig. 2 was conducted twice. A spherical cap with an angle, ϕ_o, of 15 and 30 degrees, was analyzed. Because of axial symmetry, a wedge with five degrees polar angle was employed in this work (see Fig. 2). The finite element model consisted of a number of triangular shell elements (STIF 48 in the ANSYS element library) with material and geometric nonlinear capability. The element size was restricted to $\sqrt{rt}/2$ within the loaded area while this was gradually increased toward the outer edge The element aspect ratio was kept less than two. Twenty-five and 39 elements were used for the 15 and 30 degree spherical cap, respectively. The conditions of symmetry were imposed at each boundary. Meridional displacements at the outer edge were restrained against tangential motion. A constant time step of 100 μsec was used to perform the numerical intergration and the solution was carried out until the first zero velocity peak of the structural response (maximum circumferential membrane strain) was reached. The solution of the 30 degrees spherical cap provided a slight increase in the normal displacement at the crown, while the circumferential membrane strain was decreased by about five percent. Figure 11 illus-

trates the profiles of the normal displacement for the different finite element models. Since these differences are insignificant, the use of an angle, ϕ_0, of 15 degrees is adequate. In other words, one can model a spherical shell for the nonlinear finite element analysis using only an arc with an angle of five$\sqrt{t/r}$ beyond the zone of the influence of the boundaries, i.e., beyond the loaded area.

Another study was conducted to investigate the effect of the pulse shape on the results. The spherical cap with the fifteen degrees angle and with the geometric and material parameters mentioned above was analyzed again with an applied pressure versus time input and a zero initial conditions. A triangular load-time history with a maximum peak pressure of 2470 psi (17.04 MN/m^2)(see Fig. 12) and a duration time of 500 μsec was used. This pressure-time pulse results in the same impulse used in the previous pure impulse solution. For the triangular pressure-time pulse solution, a time step size of 12.5 μsec was used during the pulse rise time. During the pulse decay time, the time step increments were increased to 25 and then to 50 μsec. This was done: (1) to characterize the input pressure-time relation, and (2) to keep the ratio of any consecutive step sizes within a value of two which is recommended in (26). The time step was then increased to 100 μsec (the same as the pure impulse case) after the pulse stopped. The results were found to agree with the pure impulse solution. The pressure-time solution results in a decrease of nine and three percent in the maximum circumferential strain and crown displacement, respectively. Figure 11

illustrates the deformed shape of the spherical shell. Notice the similarity in the deflected shape for the pressure-time and the pure impulse solution. In this study, the pure impulse loading will be employed.

Numerical integration (step-by-step) techniques are used to solve the structural dynamic equilibrium equation. The selection of the time step, Δt, has an important effect on the finite element results. In order to predict the system dynamic response accurately and to insure stability of the numerical integration, Δt has to be sufficiently small. This is particularly important if the structure is subjected to short duration loads where a large number of modes are excited or in cases involving wave propagation effects, such as the present problem.

A Houblet integration scheme (26,28) is employed in the ANSYS program to handle the numerical integration problem. Reference 24 presents a relationship between the time step size and the numerical error in the amplitude of response, expressed in terms of energy loss. For example, a 30 point per cycle integration scheme results in a numerical damping of approximately one percent. Numerical damping refers to the decay in vibration amplitude caused by the use of time steps which are large relative to the period. In wave propagation problems such as this in which reflection and refraction occur, a suggested value of Δt (29,30) is given as:

$$\Delta t < \frac{\Delta x}{c} \qquad \text{(A-1)}$$

Despite the fact that Eq. A-1 yields a small time step size, Ref. (24) recommends using

$$\Delta t < \frac{\Delta x}{3c} \tag{A-2}$$

where Δx is the smallest length of the element and c is the speed of wave propagation and is given as:

$$c = \sqrt{\frac{E}{\rho}} \tag{A-3}$$

in which ρ is the mass density. Even though Eq. A-1 results in a very small time interval, Ref. 16 recommends solving this type of problem several times using different time step sizes and selecting the "best answer". Also, Refs. 16 and 31 suggest changing the time interval during the solution until acceptable results are reached. The latter option is not automatically available in the ANSYS computer program.

The spherical cap considered above (r = 1000 in., r/t = 2400) subjected to pure impulse (v_0 = 2000 in/sec.) was analyzed using different values of the time step size Δt. The solution was performed using Δt of 100, 50 and 25 μsec, respectively. Equations A-1 and A-2 yield a maximum value of Δt of 50 and 16 μsec., respectively.

The results of the maximum membrane circumferential strain and crown normal displacement are given in Table 1. The larger time step

results in smaller displacements and membrane strain. The contribution of the higher modes is numerically filtered out (numerical damping) since the time step is large relative to the period of the higher modes (24). In this problem, the higher modes correspond to the in-plane wave propagation modes. Figure 13 illustrates the effects of the decreasing time step size on the variation of the circumferential membrane strain.

Profiles of the normalized tangential displacements are shown in Fig. 14. Each solution is normalized with respect to its maximum value. Figure 14 illustrates the differences in the tangential displacements for the three different time increments--especially near the crown. This is caused by the contribution of the higher membrane modes. Such modes are filtered out with the larger time step. These differences in the tangential displacement and its gradient introduce differences in the predicted strain (see the strain displacement relationships in Eq. 1).

To predict accurate results, one should use a smaller and smaller time step size until a converged solution is obtained. This would be extremely expensive in terms of computer time. An alternative is to use the procedure suggested in Ref. 16. Such an approach is adopted herein. The problem will be solved at least twice using different time step sizes and the results extrapolated to a time step size of zero (16).

List of Symbols

The following symbols are used in this part:

a,b = major and minor ellipse radii, respectively;

A,B = nondimensional quantities;

A_o = area over which the load is applied;

A_d = area of the deformed shape;

c = speed of wave propagation;

C = proportionality constants;

E = Young's modulus;

f_θ, f_ϕ = circumferential and meridional membrane stresses, respectively;

F_y = material yield strength;

F^* = equivalent force;

i = impulse per unit area;

I^* = equivalent impulse;

K^* = equivalent spring stiffness;

m = shell skin mass per unit area;

M^* = equivalent mass;

r = shell radius;

s_o = radius of the loaded area;

t = thickness;

T = kinetic energy;

u = meridional displacement;

U_e = internal elastic energy;

U = internal strain energy;

v = circumferential displacements;

w = displacement perpendicular to the shell surface;

w_0 = maximum radial displacement;

$\varepsilon_\theta, \varepsilon_\phi$ = circumferential and meridional strains, respectively;

$\varepsilon_{\theta_0}, \varepsilon_{\phi_0}$ = maximum circumferential and meridional strains, respectively;

ε_y = material yield strain;

$\gamma_{\theta\phi}$ = shear strain;

β_0 = half of the central angle of the loaded area;

ϕ_0 = half the central angle of the shell used;

λ = strain ductility factor;

ψ = nondimensional value;

ρ = mass density;

Δt = integration time step size.

References

1. Bath, K. J., Ramm., E. and Wilson, E. L. "Finite element formulations for large deformation dynamic analysis." International Journal Numerical Methods Engineering, 9 (1975), 353-386.

2. Klein, S. "The nonlinear dynamic analysis of shells of revolution by finite element method." Journal of Pressure Vessel Technology, 97 (March 1975), 163-171.

3. Nagarajan, S. and Popov, E. P. "Nonlinear dynamic analysis of axisymmetric shells." International Journal of Numerical Methods Engineering, 9 (1975), 535-550.

4. Harzmann, M. "Comparison of calculated static and dynamic collapse pressure of clamped spherical domes." AIAA Journal, 12 (April 1974), 568-570.

5. Ishizaki, T. and Bathe, K. "On finite element large displacement and elastic plastic dynamic analysis of shell structures." Journal of Computers and Structures, 12 (1980), 309-318.

6. Leech, J. W., Witmer, E. A. and Pain, H. H. "Numerical calculation technique for large elastic plastic transient deformation of thin shells." AIAA Journal, 6 (Dec. 1968), 2352-2359.

7. Wesenberg, D. L. "Elastic-plastic buckling of aluminum cylindrical shells subjected to axisymmetric impulse loads." Journal of Applied Mechanics, 41 (April 1974), 985-988.

8. Richard, W. H. and Witmer, E. A. "The dynamic response of cylindrical shells including geometric and material nonlinearities." International Journal of Solids Structures, 10 (1974), 243-260.

9. Lindberg, H. E. and Kennedy, T. C. "Dynamic plastic pulse buckling beyond strain-rate reversal." Journal of Applied Mechanics, 42 (June 1975), 411-416.

10. Witmer, E. A. "Large dynamic deformations of beams, rings, plates and shells." AIAA Journal, 1 (Aug. 1963), 1848-1857.

11. Richard, W. H. and Witmer, E. A. "Finite element analysis of large elastic-plastic transient deformation of simple structures." AIAA Journal, 9 (Sept. 1971), 1719-1724.

12. Von Riesemann, W. A., Haisler, W. E. and Stricklin, J. A. "Large deflection elastic-plastic dynamic response of stiffened shells of revolution." Journal of Pressure Vessel Technology, 96 (May 1974), 87-95.

13. Forrestal, M. J., Tucker, W. K. and von Riesemann, W. A. "Impulse loading of finite cylindrical shells." AIAA Journal, 13 (Oct. 1975), 1396-1398.

14. Symonds, P. S. "Large plastic deformations of beams under blast type loadings." Proceedings, 2nd U.S. National Congress of Applied Mechanics (1954), 505-515.

15. Duffey, T. A. and Krieg, R. D. "The effects of strain hardening and strain-rate sensitivity on the transient reponse of elastic plastic rings and cylinders." International Journal of Mechanical Science, 11 (1969), 825-844.

16. Armen, H. and Garnet, H. "Finite element analysis of elastic-plastic wave propagation effects." Journal of Computers and Structure, 6 (1976), 45-53.

17. Desai, C. S. Elementary Finite Element Method. Englewood Cliffs, New Jersey:Prentice Hall, 1979.

18. Hartzman, M. "Nonlinear dynamic of solids by finite element method." Journal of Computers and Structure (1972), 47-77.

19. Biggs, J. M. Introduction to Structural Dynamics. New York: McGraw Hill Book Company, Inc., 1964.

20. Clough, R. W. and Penzien, J. Dynamics of Structures. New York: McGraw Hill Book Company, Inc., 1975.

21. Baker, E. H., Cappel, A. P., Kovalesvsky, L. and Verehe, R. M. Shell Analysis Manual. Springfield, Virginia:NASA CR-912, Clearing House for Federal Scientific and Technical Information, N68-24802, 1968.

22. Ford, H. and Alexander, J. M. Advanced Mechanics of Materials. 2nd ed. New York:John Wiley and Sons, Inc., 1974.

23. Szilard, R. "Theory and analysis of plates." Classical and Numerical Methods. Englewood Cliffs, New Jersey:Prentice-Hall, Inc., 1974.

24. ANSYS Engineering Analysis System. User's Manual. Houston, Pa.: Swanson Analysis System, Inc., 1979.

25. Zienkiewicz, O. C. The Finite Element Method. 3rd ed., New York: McGraw Hill Book Company, Inc., 1977.

26. Kohnke, P. C. ANSYS Theoretical Manual. Houston, Pa.:Swanson Analysis System, Inc., 1979.

27. Roark, P. C., and Young, W. C. Formulas for Stress and Strain. 5th ed. New York:McGraw Hill Book Company, Inc., 1975.

28. Wilson, E. L. and Bathe, K. J. Numerical Methods in Finite Element Analysis. Englewood Cliffs, New Jersey:Prentice Hall, Inc., 1976.

29. Desai, C. S. Elementary Finite Element Method. Englewood Cliffs, N.J.:Prentice-Hall, Inc., 1979.

30. Hadala, P. E. and Taylor, H. M. "Effect of grid size on cutoff frequency in numerical solution of an elastic one dimensional wave propagation problem." U. S. Army Engineering Division, Huntsville Technical Report S-72-2, 1972.

31. Garnet, H. and Armen, H. "A variable time step method for determining plastic stress reflection from boundaries." AIAA Journal, 13 (April 1975), 45-53.

Table 1. Summary of the finite element and approximate results

Structure	v_o in./sec	Δt μsec.	ε^a max in./in.	ε^b $\Delta t \simeq 0$ in./in.	δ^c max in.	δ^b $\Delta t \simeq 0$ in.	λ^d F.E.	λ^e	cpu time hr.
sphere		100	.0120		8.7				1.3
				.018		9.9	10.8		
R/t=2400	2000	50	.0150		9.3			13.8	2.4
				.019		10.1	11.4		
		25	.0170		9.7				5.5
sphere		100	.0040		4.2				1.3
	1000			.0054		4.6	3.25	3.8	
R/t=2400		50	.0047		4.4				2.4
sphere		100	.0110		8.7				1.3
	2000			.0164		9.9	10	13.8	
R/t=1200		50	.0154		9.3				2.4
cylinder		100	.0125		10.2				5.8
	2000			.0183		11.4	11	13.8	
R/t=1200		50	.0154		10.8				11.0
		100	.0097		11.8				1.3
plate				.0145		13.2	8.7		
	2000	50	.0121		12.5			13.8	2.4
t=.833"				.0161		14.5	9.7		
		25	.0141		13				5.5

[a]Maximum circumferential membrane strain.

[b]Extrapolated answers.

[c]Crown radial displacement.

[d]Finite element results: $\lambda_{F.E.} = \frac{\varepsilon @ \Delta t \simeq 0}{\varepsilon_y}$.

[e]Ductility factor calculated using Equation 39.

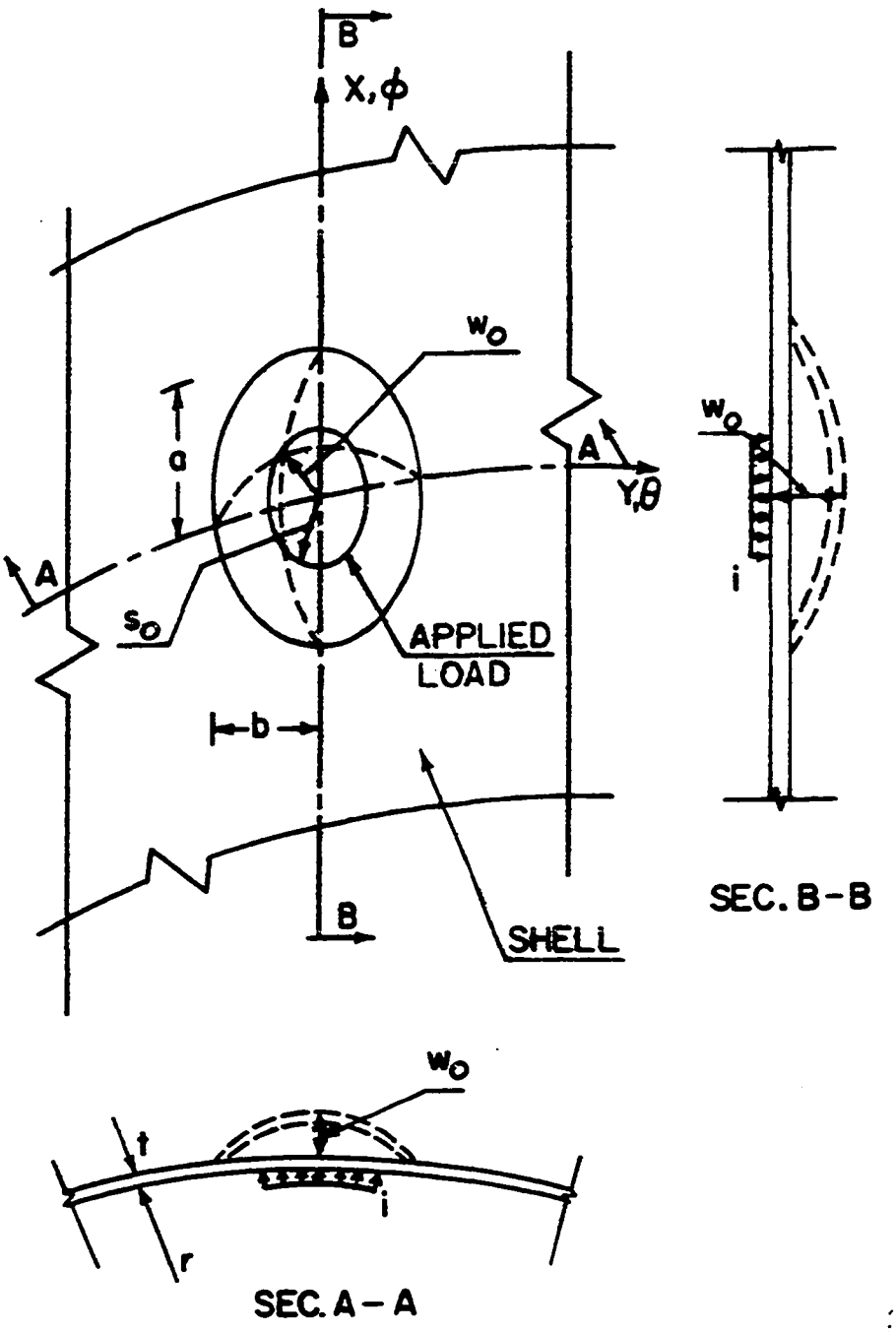

Figure 1. Deformed shape-localized loaded cylindrical shell

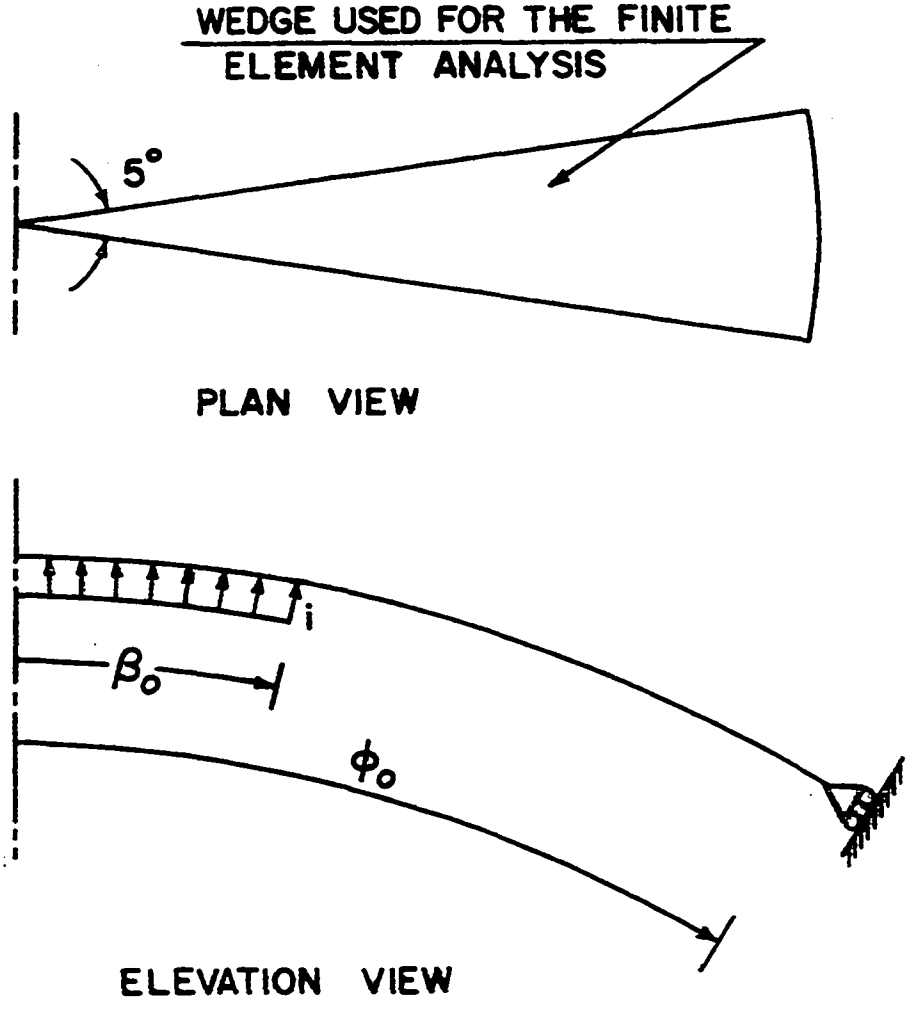

Figure 2. Hemispherical cap with localized dynamic pressure

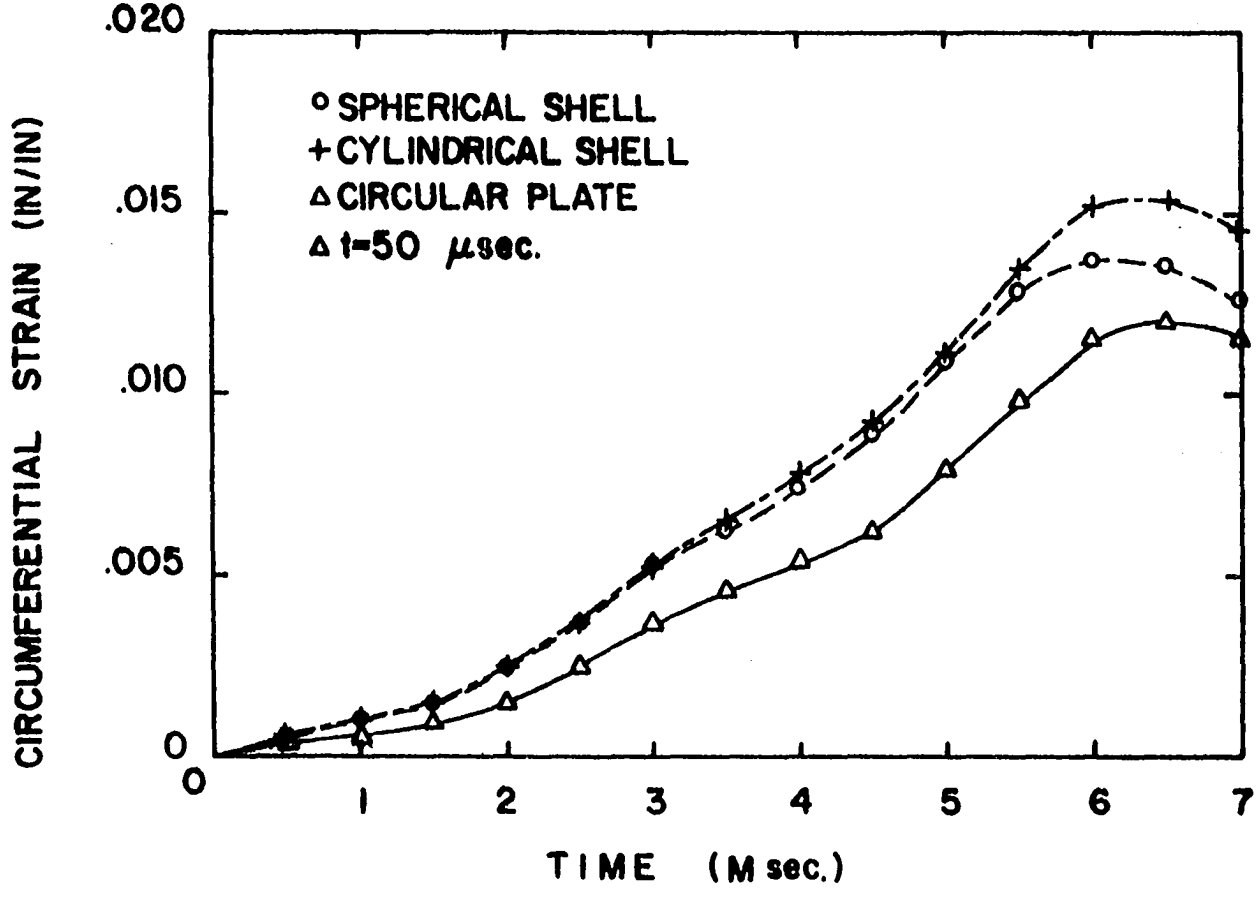

Figure 3. Circumferential membrane strain versus time

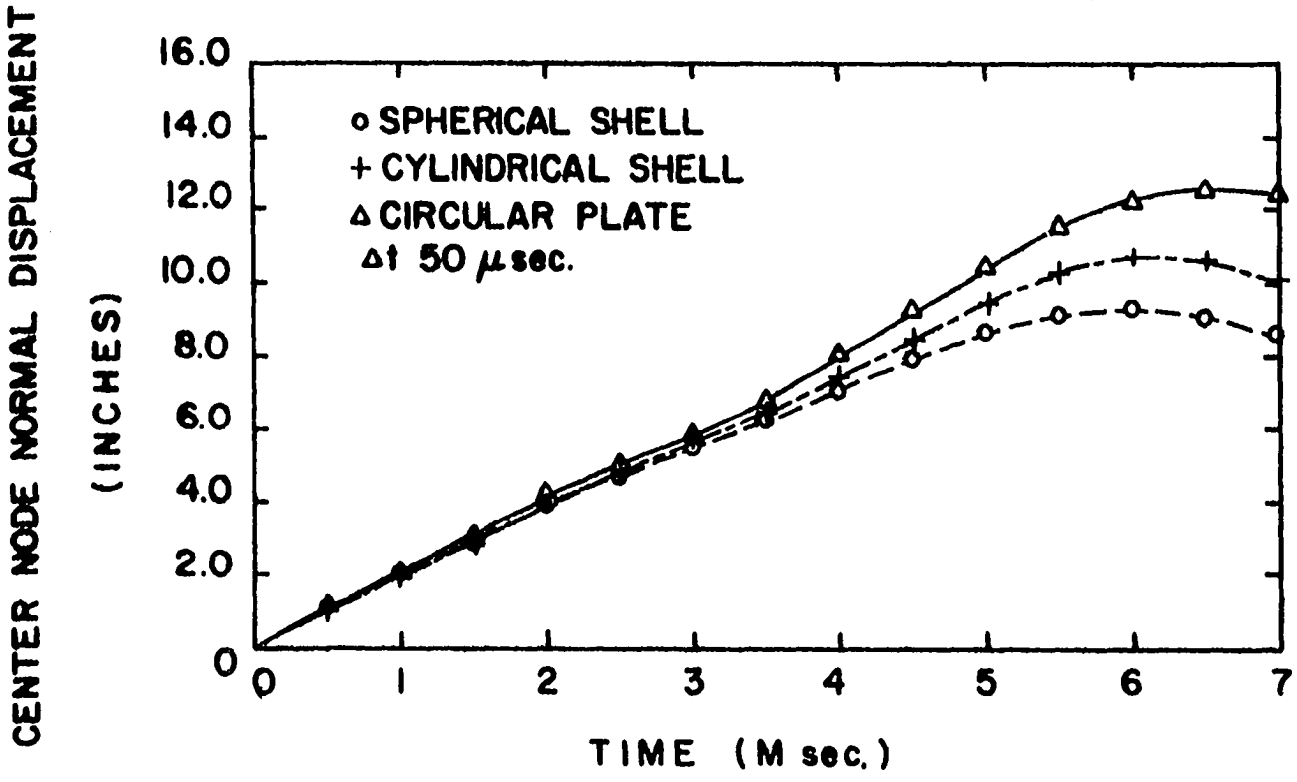

Figure 4. Center node normal displacement versus time

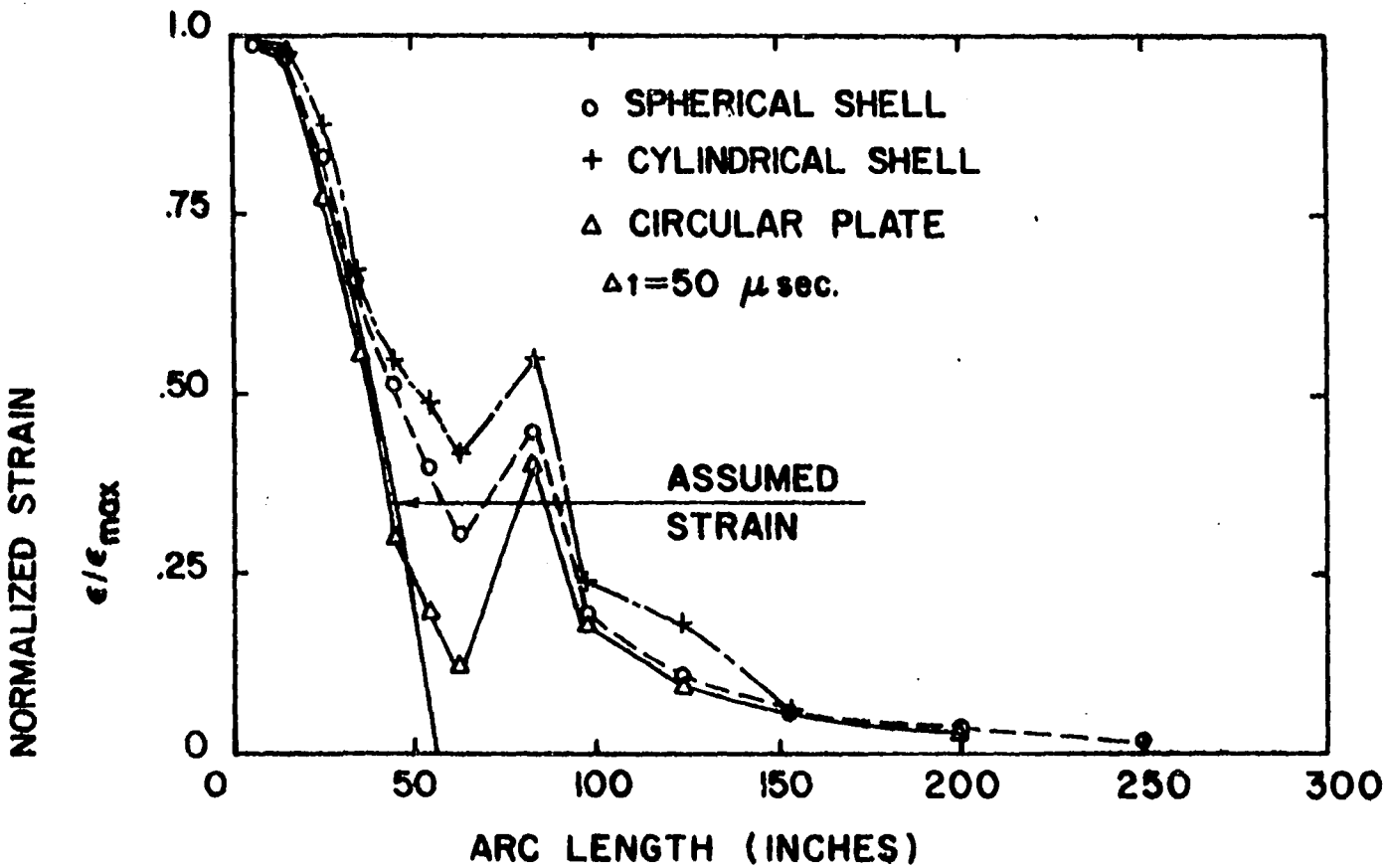

Figure 5. Normalized circumferential strain versus arc length

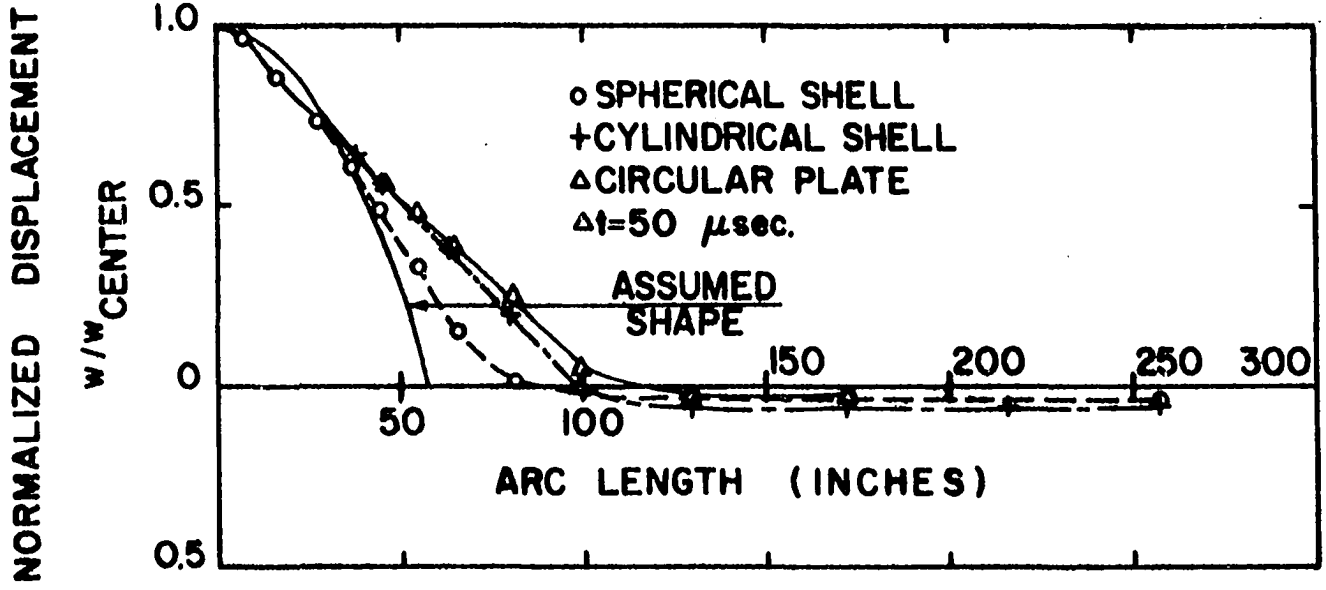

Figure 6. Normalized radial displacement versus arc length

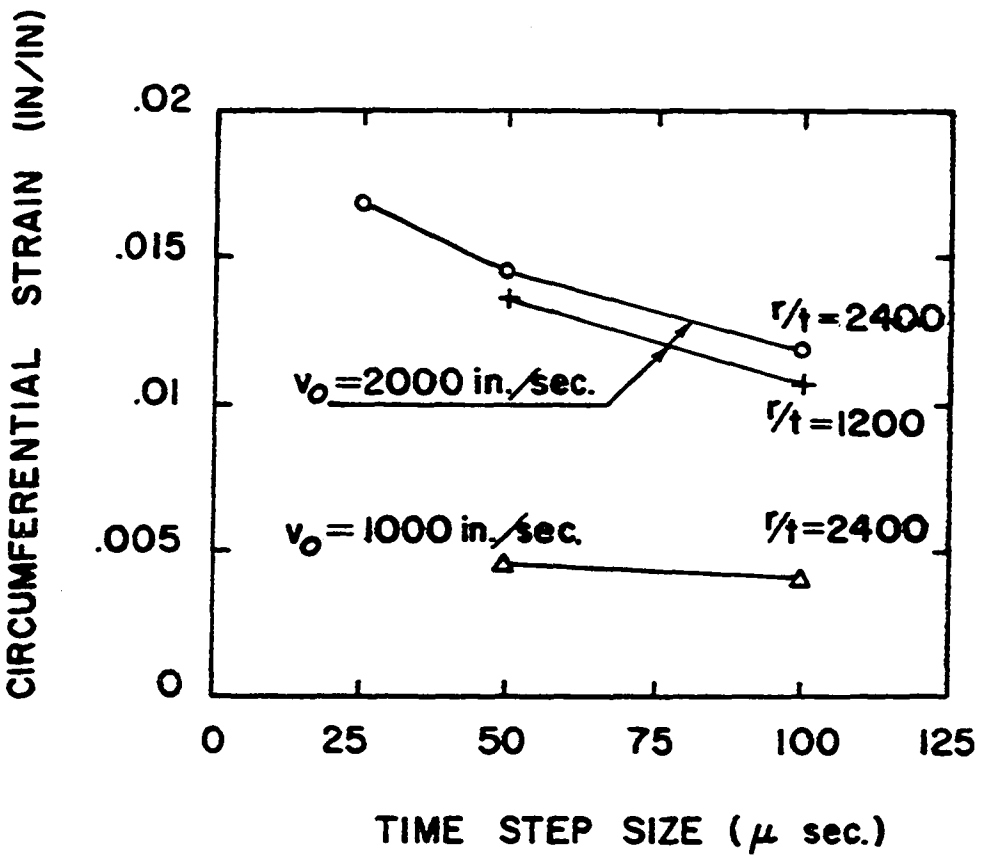

Figure 7. Circumferential membrane strain versus time step size (spherical shell, r = 1000")

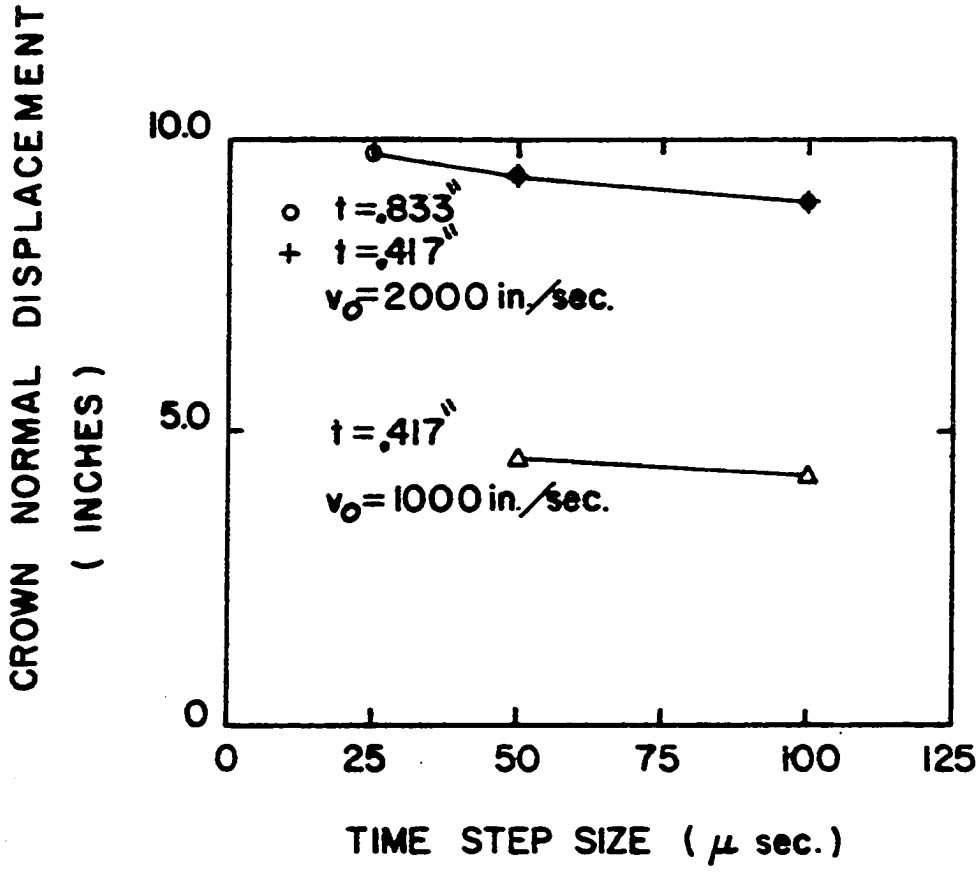

Figure 8. Crown normal displacement versus time step size (spherical cap, r = 1000")

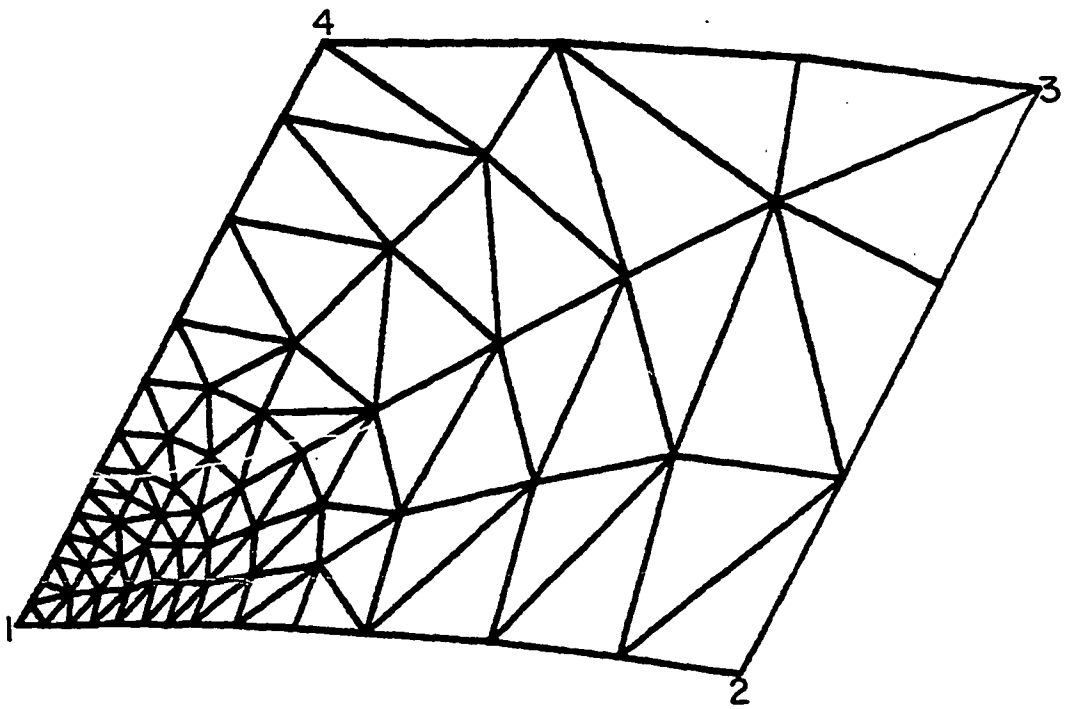

Figure 9. Finite element mesh used for the cylindrical shell problem

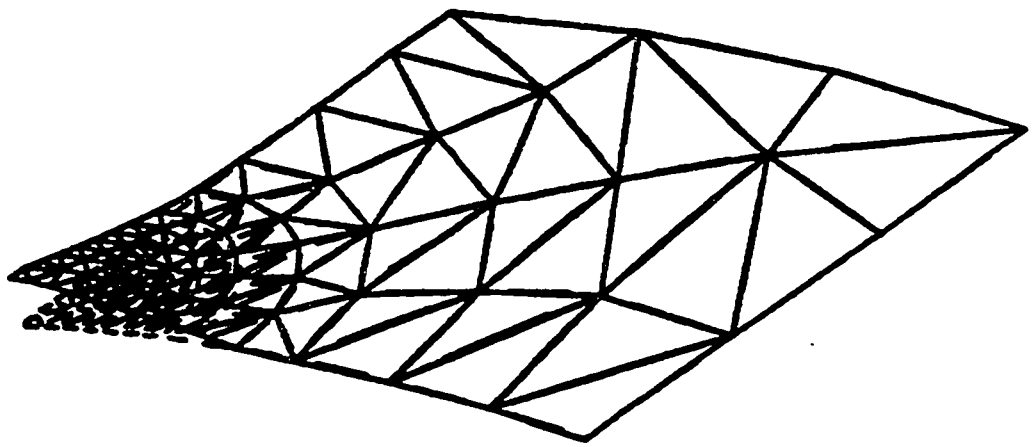

Figure 10. Deformed shape of the cylindrical shell problem

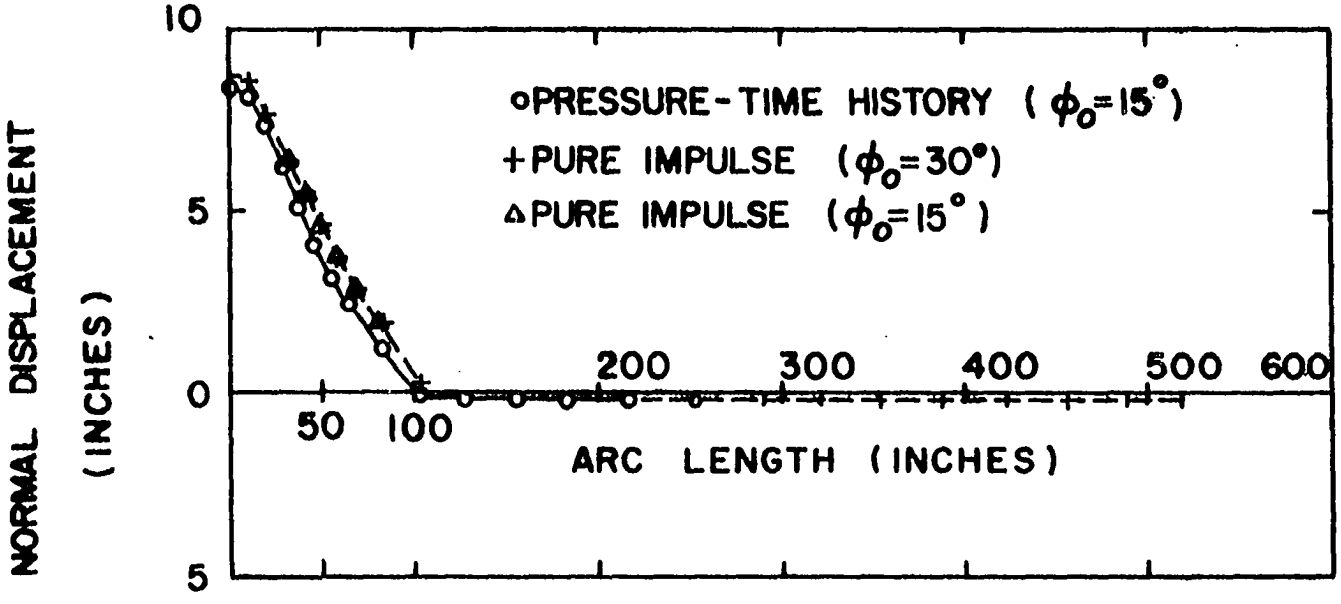

Figure 11. Normal displacement versus arc length for different loading

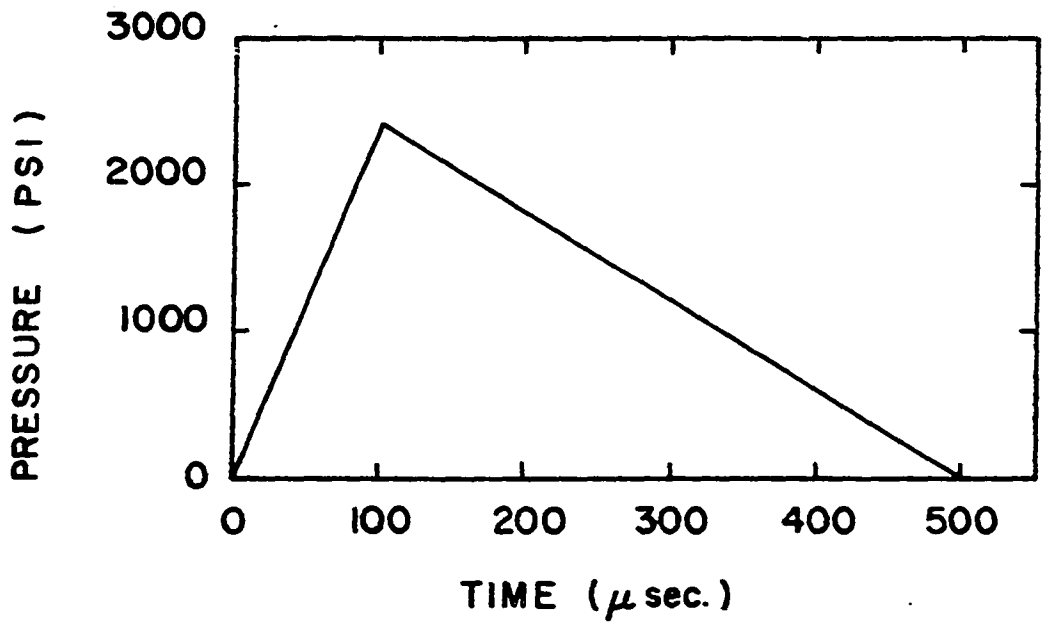

Figure 12. Pressure-time relationship used in pulse shape study

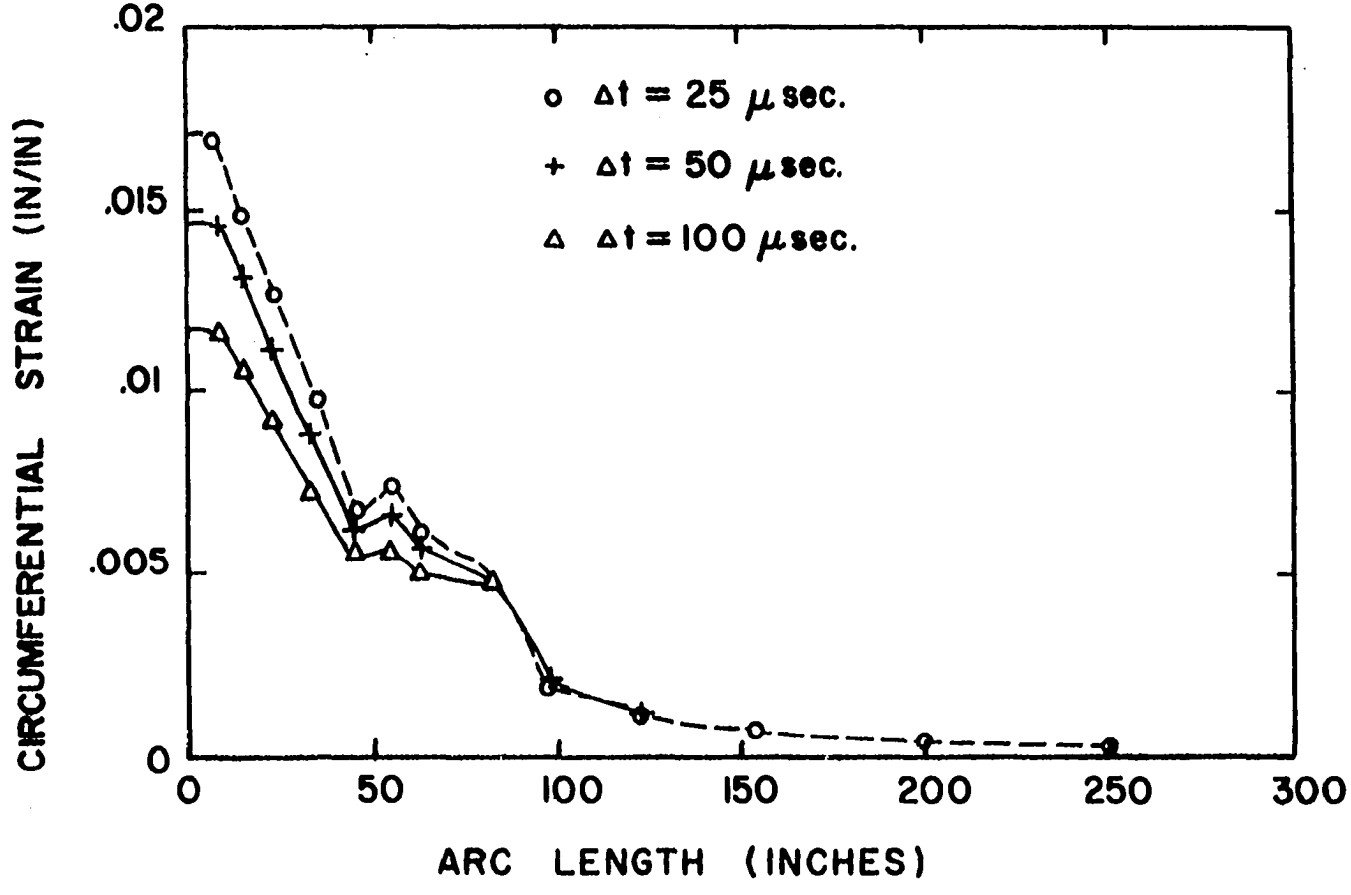

Figure 13. Circumferential membrane strain versus arc length for the spherical shell used in time step study

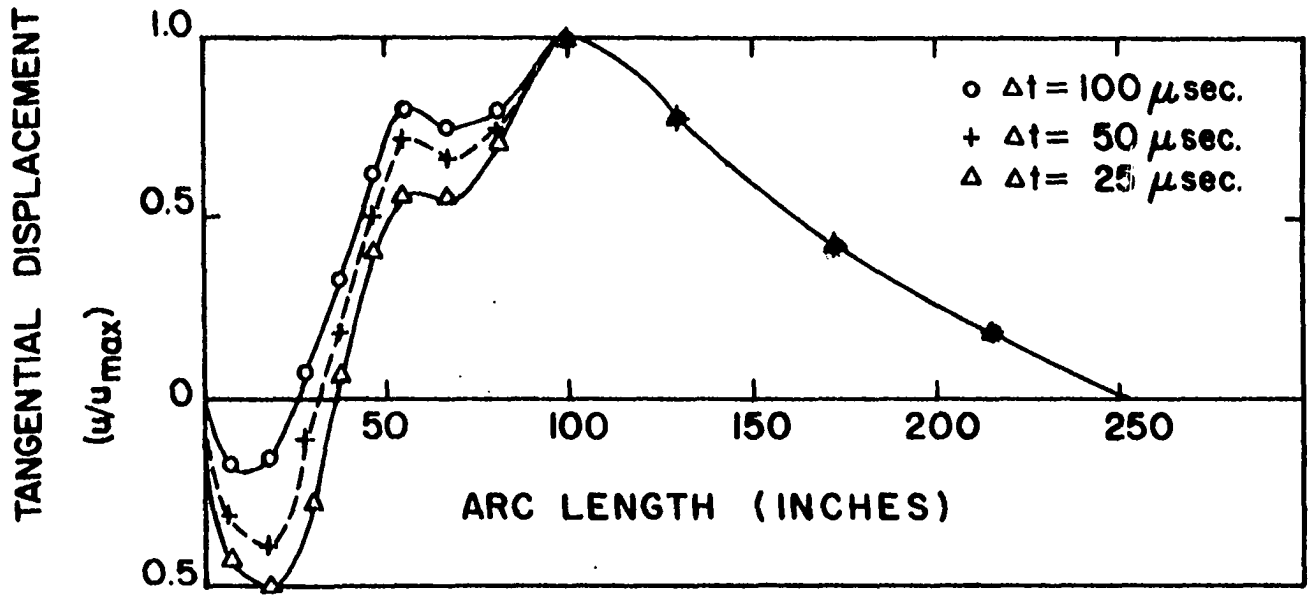

Figure 14. Normalized tangential displacement versus arc length for the spherical shell used in the time step study

PART III. RELIABILITY ASSESSMENT OF CONTAINMENT RESISTANCE

Abstract

The purpose of the containment vessel in a nuclear power plant is to prevent the release to the atmosphere of any radioactivity which may accidentally be present within the vessel. In spite of the extreme precautions that are considered in the design and construction procedures, leakage of radioactivity still does have a small probability of occurrence. To study the probability of such an event, a best estimate and uncertainty assessment of the containment resistance is needed. In this paper three reliability assessments: an advanced second moment method, a Monte Carlo simulation technique and a simplified approach for practical analysis, are proposed. Criteria for the prediction of the theoretical resistance of stiffened cylindrical shells and ellipsoidial heads under uniform internal static pressure are presented. The statistical characterization of the containment resistance is performed using these criteria in conjunction with the three reliability assessment techniques. A numerical example is presented to illustrate the differences among the reliability approaches.

Introduction

Criteria for structural design have generally been based on the traditional safety factor concept. These criteria may differ in the levels of safety they provide because of the difference in the design philosophy and the assumptions involved. Even with the presence of a safety factor, there is a small probability that an adverse event, or

failure, can occur because of the uncertainties arising from randomness in design variables such as geometric parameters, material strength and applied loads. Uncertainties in the mathematical model used in the prediction of the structure resistance should also be considered. Therefore, the problem of structural design must be resolved in light of a best estimate and uncertainty assessment. Such conclusions have led to the application of probabilistic methods to structural design (1,2,3,4,5).

This paper is part of a study the objective of which is to assess the uncertainty of the containment vessel resistance for some nuclear power plants. It summarizes some reliability techniques and demonstrates the use of such techniques to assess the uncertainty in the prediction of the containment vessel resistance.

Evaluation of Reliability Analysis

The conceptual framework of reliability is provided by classical reliability theory as described in (1,3). The reliability of a structure may be calculated in terms of the probability density functions of the random resistance and load variables. In principle, there are three different levels of sophistication for the reliability-based design approach. The Level 1 method is defined as design and safety checking aspects whose reliability is provided by introducing a set of partial safety factors applied to the nominal values of the basic design variables. These factors are statistical parameters that are deduced from probabilistic considerations to arrive at an appropriate

level of structural reliability. The second level, referred to as the Level 2 method, employs safety checks at a selected number of points (often one point only) of the safety domain boundaries. Probability density functions for the design random variables are not required for Level 2 analysis. Performance of Level 2 reliability analysis necessitates the first two moments, i.e., the mean and standard deviation, of each variable. The reliability is measured by what is called a safety index, β. (In some studies, β is known as a reliability index.) Level 3 is the most complete reliability technique. All joint probability distributions of all design variables involved must be known; and the necessary integration, usually multidimensional, of the joint probability density functions of the variables must be computed. These operations are certainly not easy to perform; however, Level 3 is the only available means to check the validity of Level 2 and Level 1 analyses.

Reliability Analysis

As previously stated, the probability of failure may be computed using the probability density functions of the random resistance and load variables. In general, these variables are also functions of many other variables, and in real problems, the information available is not explicitly given. The work presented herein is devoted to finding the probabilistic characteristics of the structural resistance variable R. Let R be a function of the independent variables X_i, i.e.,

$R = R(X_1, X_2, \ldots X_n)$, then by definition, the cumulative distribution $F_R(.)$ for a selected value, r, can be written as:

$$F_R(r) = P(R \leq r) = P\ (R(X_1, X_2 \ldots X_n) \leq r) \qquad (1)$$

or

$$F_R(r) = \int \ldots \int \ldots \int f_{\underline{X}}(x_1, x_2 \ldots x_n) dx_1 \ldots dx_n \qquad (2)$$

in which $f_{\underline{X}}(x_1, x_2 \ldots x_n)$ is the probability density function of the independent variables X_i and x_i represents a specific value of X_i. The evaluation of the integral in Eq. (2) is difficult and impractical except for simple functions with not more than three variables (6). However, simulation techniques (7) can be used to perform such an evaluation. These difficulties have motivated the development of Level 2 reliability analysis. In this paper, second moment methods and Monte Carlo simulation technique are employed to conduct Levels 2 and 3, reliability assessments of the containment vessel resistance.

Second moment method (Level 2)

In this approach, the uncertainty of the random variables X_i is characterized by their first two moments of the perhaps unknown probability density functions. The fundamental operational procedures were introduced by Cornell (8) and their philosophical bases are presented in (9,10). This reliability concept is referred to as the mean first order second moment method (MFOSM) and is summarized as follows:

Let $R = R(X_1, X_2 \ldots X_n)$ be the structural resistance, which is a function of the random variables X_i. This function has to be linearized at some points for the purpose of performing the reliability analysis. In the MFOSM method, these points were selected to be the mean values, $\bar{x}_i$, of the random variable X_i. Therefore, linearization of this function using Taylor series and neglecting the nonlinear terms yields

$$R \simeq R(\bar{x}_1, \bar{x}_2 \ldots \bar{x}_n) + \sum_{i=1}^{n} (X_i - \bar{x}_i) \frac{\partial R}{\partial X_i}\Bigg|_{X_i = \bar{x}_i} \tag{3}$$

When the random variables X_i are independent, i.e., the correlation coefficients are zeros, the mean and variance of R become

$$\bar{R} = R(\bar{x}_1, \bar{x}_2 \ldots \bar{x}_n) \tag{4}$$

$$\sigma_R^2 = \sum_{i=1}^{n} \left(\frac{\partial R}{\partial X_i}\right)^2 \Bigg|_{X_i = \bar{x}_i} \sigma_{X_i}^2 \tag{5}$$

Assuming a normal distribution for R, the safety index, β, is

$$\beta = \frac{\bar{R} - r}{\sigma_R} \tag{6}$$

Despite its simplicity and practical advantages, there is some criticism about the mean first order second moment method. The

criticism is against the linearization of the limit state function (R-r, in this case) at the mean value, which may result in significant errors. Also, the MFOSM method fails to be invariant for different equivalent mathematical formulations of the same problem (10,11). Because of these drawbacks, other forms of the second moment theory have been developed (12,13).

Several investigators (10,12,13) have shown that a better linearization is obtained at what is called the design point. Linearization of the limit state at such a point insures the invariance of the statistical characteristics of the function under any mathematical formulation. This approach is known as invariant or advanced second moment method. The general formulation of this concept consists of two steps: (1) transforming the random variables, X_i, into a space of uncorrelated normalized variables, u_i, in which

$$u_i = \frac{X_i - \bar{x}_i}{\sigma_{X_i}} \tag{7}$$

(2) measuring the shortest distance between the origin of the transformed space to the failure surface. The point $(u_1^* \; u_2^*, \ldots \quad u_n^*)$ on this surface which corresponds to the shortest distance is called the design point, and the minimization problem can be stated as:

$$\beta = \min. \sqrt{\sum_{i=1}^{n} u_i^2} \tag{8}$$

with constraint,

$$R(u_1,u_2\ldots u_n)-r=0 \tag{9}$$

or, in the basic variable X_i, where the design point is identified as $(x_1^*,x_2^*\ldots x_n^*)$,

$$\beta = \min. \sqrt{\sum_{i=1}^{n} \left(\frac{X_i - \bar{x}_i}{\sigma_{X_i}}\right)^2} \tag{10}$$

with constraint,

$$R(X_1,X_2\ldots X_n)-r=0 \tag{11}$$

The cumulative distribution of R, denoted by $F_R(.)$ can be approximated as:

$$F_R(.) = P(R<r) = \Phi(-\beta) \tag{12}$$

in which $\Phi(.)$ is the cumulative distribution of the standard normal distribution.

Equation 12 yields the exact cumulative distribution when the boundary of the transformed failure region is linear and R is normally

distributed. However, when the boundary surface of the transformed failure region is nonlinear, it is not correct to assume that the cumulative distribution is exact. For example, if the boundary surface of $R(u_1,u_2, \ldots, u_n)-r=o$, in the transformed space, is concave toward the origin, Eq. 12 underestimates $F_R(r)$, whereas, if the boundary surface is concave away from the origin of the transformed space, Eq. 12 overestimates the cumulative distribution. In real structure problems, at least some of the variables are non-normal; for example, material yield strength is described as lognormally distributed (11), and relatively small live loads seem to have a Gamma distribution (10). However, these non-normal distribution types can be transformed into equivalent normal variables by the methods outlined in (6,10,13). This transformation is accomplished by using a Taylor Series expansion of the non-normal distribution about the design point x_i^*.

$$x_i^N = x_i^* - \phi[F_i(x_i^*)]\ \sigma_i^N \tag{13}$$

$$\sigma_i^N = \frac{\phi\{\Phi^{-1}[F_i(x_i^*)]\}}{f_i(x_i^*)} \tag{14}$$

where $\bar{x}_i^N$, σ_i^N are the mean and standard deviation of the equivalent normal distribution, and $f_i(.)$ and $F_i(.)$ denote the probability density and the cumulative distribution of X_i, and $\phi(.)$ is the density function for the standard normal variate.

Monte Carlo simulation technique (Level 3)

As noted before, Level 3 analysis requires performing multidimensional integration of the probability density functions of the random variable, X_i. In the presence of such a difficult integration, the only practical approach is the direct simulation of the random process. The simulation approach consists of drawing samples of the independent input variables according to their probability distribution and then feeding them into the mathematical model to estimate the statistical characteristics of the dependent function.

An approximation to the cumulative distribution can be obtained using the Monte Carlo simulation technique in conjunction with the Order Statistic Concept (14). Since R is a function of the other random variables, X_i, one can generate, by means of random number generation, random values of X_i, which are then substituted into the resistance equation to predict R. This process is repeated until a satisfactory number of observations, say N times, is attained. The outcome results, R_1 through R_N, are then rearranged in increasing order of magnitude $R^{(1)}$, $R^{(2)}$,... $R^{(N)}$ which is defined to be order statistic. This rearrangement is helpful when searching for a specific value of R. Now the probability that R is less than a specific value, say, r, can be approximated by the fraction of times that this event occurred, i.e.,

$$P(R < r) = F_R(r) \simeq \frac{j}{N}; \qquad N = \text{very large number} \qquad (15)$$

in which j is the jth occurrence of such an event in N number of observations.

Structure Resistance Modes

A structure generally has more than one possible independent resistance mode which decreases the overall reliability of the structure. The failure of such a structure can be conservatively modeled by taking the resistance modes to form a series system, i.e., unsatisfactory performance in any mode will cause the structure to fail. For a structure with m possible resistance modes, the system resistance, R, is defined as the minimum of the individual mode resistances, R_k; k=1,2, ...m. The system resistance cumulative distribution, $F_R(r)$, can be computed by Monte Carlo simulation or the advanced second moment method. Using the previously discussed simulation, one can predict the resistance of the possible modes, which then is used in conjunction with the order statistic (14) to calculate $F_R(r)$. In the advanced second moment approach, Ref. (15) gives the bounds of the cumulative distribution $F_R(r)$ as:

$$\text{Max.}\ (F_{R_k}(r)) \leq F_R(r) \leq 1 - \prod_{k=1}^{m} (1-F_{R_k}(r)) \qquad (16)$$

The lower bound assumes perfect correlation of the resistances R_i, while the upper bound assumes statistical independence. If $F_{Rk}(r)$ are sufficiently small, then the upper bound becomes

$$F_R(r) \leq \sum_{k=1}^{m} F_{R_k}(r) \qquad (17)$$

Bounds of the structure safety index, $\beta(r)$, are calculated using Eq. 16 and

$$\beta(r) = \Phi^{-1}[1 - F_R(r)] \qquad (18)$$

Numerical Example

In the following discussion, an example problem is solved to illustrate the differences between the advanced second moment method (Level 2) and the Monte Carlo simulation technique (Level 3).

Consider the (imaginary) stiffened containment with a true 2:1 ellipsoidal head, as shown in Fig. 1, under uniform internal static pressure. The containment is fairly typical. The vessel can be considered as a number of ring panels framed by the circumferential stiffeners. Therefore, the possible resistance modes for the cylinder can be identified as general and inter-ring modes. An asymmetric buckling mode or an axisymmetric limit pressure mode can occur in the containment head. Criteria for the prediction of the theoretical resistance, R_t, for these modes under uniform internal static pressure are given in the Appendix.

In-service resistance, R, is related to the theoretical resistance throughout a factor, X_o, referred to as modeling error. This factor must be considered in the uncertainty assessment analysis as one of the containment resistance random variables and can be expressed as:

$$X_0 = \delta \Delta \tag{19}$$

where δ represents the basic variability of the theoretical resistance with respect to experimental results, while the factor Δ accounts for the variability between experimental results and in-service conditions. Typical values of the statistical characteristics of the factor Δ are given by other investigators (1,16), while the mean and coefficient of variation (c.o.v.) of the factor δ are given for 95% confidence in Ref. 17. The statistical parameters and the distribution type of the random variables involved in the containment resistance reliability analysis are given in Table 1. The source of these data is Ref. 17, which considered the containment thickness as random but uniform.

The reliability analysis of the containment resistance performed by the Monte Carlo simulation assumed that the random variables are independent among the various failure modes. In other words, random numbers for each variable were generated independently for each mode of failure even though the variable may have the same nominal value in two or more of the failure modes. The results of the reliability assessment of the containment resistance are summarized in Fig. 2. As can be seen, the advanced second moment method provides upper and lower limits of the cumulative distribution of the containment vessel resistance (Eq. 16), and it is noteworthy to point out that the Monte Carlo simulation solution is within this range.

Simplified Reliability Approach

Intuitively, one would expect that if the coefficient of variation of a particular random parameter, X_i, is relatively small, the analysis would not be affected by this parameter. This is evident when the Taylor series expansion about the design point is examined. In particular, the coefficient of variation of the geometric parameters are significantly smaller than the c.o.v. of the material yield strength and the modeling error (see Table 1). Therefore, to assess the uncertainty of the containment resistance, one can conceivably consider only X_o and F_y to be random variables and ignore the randomness of the other variables. In addition, since X_o and F_y are independent lognormally distributed random variables, an approximate value of the safety index, β_k, for each resistance mode can be expressed as (11,16)

$$\beta_k(r) = \frac{\ell n(R_k/r)}{\left[V_{X_o}^2 + V_{F_y}^2\right]^{1/2}} \tag{20}$$

The bounds on the containment resistance cumulative distribution and the system safety index $\beta(r)$ can then be calculated using Eqs. 16 and 18, respectively. Also, if the resistance, R ($R=\min(R_k)$), is assumed to be lognormally distributed, the corresponding coefficient of variation can be approximately calculated as:

$$V_R(r) = \frac{\ell n\ (R/r)}{\beta(r)} \tag{21}$$

This simplified approach is applied to the previous containment vessel. The resulting upper bound cumulative distribution is superimposed on the Monte Carlo simulation and advanced second moment results shown in Fig. 2. $F_R(r)$ from the Monte Carlo simulation and the simplified approach are rather close, while the results of the advanced second moment method bound both of these. This indicates that the results are relatively insensitive to the randomness of the geometric variables. Shown in Fig. 3, the results of Eq. 21 for various values of r indicate the small change of the coefficient of variation of the resistance. This implies that the containment resistance can be approximately considered lognormally distributed.

Conclusions

Criteria for predicting the resistance of stiffened cylindrical shells and ellipsoidal heads are presented. Various reliability analysis methods have been employed to define the statistical characterization of the containment resistance. Three different reliability assessments - Monte Carlo simulation, advanced second moment and a simplified approach - are proposed. A numerical example is given and the results yield the following conclusions. The Monte Carlo technique can be applied directly to assess the uncertainty of the containment resistance since explicit equations of the different resistance modes

are given. Large numbers of simulation points are required to predict an adequate statistical characterization of the vessel resistance. The advanced second moment provides upper and lower bounds of the cumulative distribution when multiple failure modes are involved. The simplified assessment approach is sufficiently accurate to define the statistical parameters of the resistance because of the insignificant effect of the randomness of the geometric variables. Such an approach can be adopted for conducting practical and preliminary uncertainty analysis if the first two moments of the yield strength and modeling error are known.

Appendix. Resistance Equations for the Containment Vessel

Criteria for the prediction of the different containment resistance modes:

A. Cylindrical Shell (18)

i - General Mode:

$$R_t = \frac{2 F_y t}{D} \left(\frac{2}{\sqrt{3}} + \frac{A_1}{s_1 t} \right) \qquad \text{(A-1)}$$

ii - Inter-Ring Mode:

$$R_t = \frac{2 F_y t}{DK} \left(\frac{2}{\sqrt{3}} + \frac{6Z D}{s_1^2 t} \right) \qquad \text{(A-2)}$$

where

$$Z = \frac{t^2}{4} + \frac{A_2 c}{s_2}$$

$$K = 1 - \frac{2 F_y D^2}{29{,}000{,}000\ s_1^2}$$

B - 2:1 Ellipsoidal Head (19)

i - Axisymmetric Limit Pressure:

$$R_t = \frac{2 F_y t}{D} \left(1 + \frac{50 F_y}{29{,}000{,}000} \right) \qquad \text{(A-3)}$$

ii - Asymmetric Buckling:

$$R_t = 10.4 F_y \left(\frac{t}{D} \right)^{1.25} \qquad \text{(A-4)}$$

List of Symbols

The following symbols are used in this part:

A_1, A_2 = circumferential stiffener and stringer cross-sectional area;

c = eccentricity of stringer centroid;

D = containment diameter;

$f(\ )$ = probability density function;

F_y = material yield strength;

$F(\ )$ = cumulative distribution;

r = specific resistance value;

R, R_k, R_t = minimum, kth mode and theoretical resistance, respectively;

s_1, s_2 = ring and stringer stiffener spacing;

t = containment wall thickness;

u_i = normalized variable;

V_{Fy}, V_R, V_{X_0} = material yield strength, resistance and modeling error coefficient of variation (c.o.v.), respectively;

X_i = random variable;

X_0 = factor relates in-service containment resistance to the containment theoretical resistance;

Z = section plastic modulus per unit length;

$\overline{\ \ }$ = denotes the mean value of the variable;

σ = standard deviation;

β_k = safety index for the ith mode;

β = structure safety index.

δ = factor represents the variability of the theoretical resistance with respect to experimental results.

Δ = factor accounts for the variability between experimental and in-service conditions.

$\phi(\ )$ = density function of the standard normal variate;

Φ = cumulative distribution of the standard normal distribution.

References

1. Ang, A. H-S. and Cornell, C. A. "Reliability Bases of Structural Safety and Design." Journal of Structural Division, 100, ST9, (Sept. 1974), 1755-1769.

2. Ang, A. H-S., "Structural Risk Analysis and Reliability Based Design." Journal of Structural Division, 99, ST9, (Sept. 1973), 1891-1910.

3. Freudental, A. M., Garrelts, J. M. and Shinozuka, M. "The Analysis of Structural Safety." Journal of Structural Division, 90, ST1, (Feb. 1966), 267-325.

4. Ravindra, M. K. and Galambus, T. V. "Load and Resistance Factor Design of Steel." Journal of Structural Division, 104, ST6, (Sept. 1978), 1337-1353.

5. Lind, N. C. "Formulation of Probabalistic Design." Journal of Engineering Mechanics, 103, EM2, (April 1977), 273-284.

6. Ezio, L. The Assessment of Structural Safety. Forest Grove, Oregon:Research Study Press, 1979.

7. Hammersley, J. M. and Handscomb, D. C. Monte Carlo Method. New York:John Wiley and Sons, Inc., 1964.

8. Cornell, C. A. "Structural Safety Specification Based on Second-Moment Reliability Analysis." ABSE Symposium, London 1969.

9. "First Order Reliability Concepts for Design Codes." Bulletin D' Information No. 112, Comite Europeen du Beton, Munich, July 1976.

10. Ellingwood, B. "Development of a Probability Based Load Criterion for American National Standard A58." National Bureau of Standards Special Publication 577, 1980.

11. Greimann, L. F., Fanous, F. S., Sabri, A., Ketelaar, D., Wolde-Tinsea, A. and Bluhm, D. "Reliability Analysis of Containment Strength," Report to U.S. NRC, NUREG/CR-1981, IS-47353 (Nov. 1980).

12. Hasofer, A. M. and Lind, N. C. "Exact and Invariant Second Moment Code Format." Journal of the Engineering Mechanic Division, 100, EM1, (Feb. 1974), 111-121.

13. Rackwitz, R. "Practical Probabilistic Approach to Design." Technical University of Munich, 1976.

14. Mood, A. M., Graybill, F. A. and Boes, D. C. Introduction to the Theory of Statistics. 3rd Ed. New York:McGraw-Hill, 1974.

15. Cornell, C. A. "Bound on the Reliability of Structural System." Journal of the Structural Division, 93, ST1, (Feb. 1967), 171-200.

16. Morales, W. J., Duke, J. M. and Mazumdar, M. "Reliability of Slightly Oval Cylindrical Shells Against Elastic-Plastic Collapse." Reliability Engineering in Pressure Vessels and Piping, ASME, San Francisco, (June 1975), 35-49.

17. Greimann, L. F., Fanous, F. S., Wolde-Tinsae, A., Ketelaar, D., Lin, T. and Bluhm, D. "Reliability Analysis of Containment Strength." Report to U.S. NRC, NUREG/CR 2442, IS-4753 (Nov. 1981).

18. Fanous, F. S. and Greimann, L. F. "Simplified Techniques for the Inelastic Analysis of Stiffened Shells Under Uniform Static Internal Pressure." Paper to be submitted to the Journal of Pressure Vessel Technology, ca. 1982.

19. Galletly, G. D. and Aylward, R. W. "Plastic Collapse and the Controlling Failure Pressure of Thin 2:1 Ellipsoidal Shells Subjected to Internal Pressure." Journal of Pressure Vessel Technology, 101, (Feb. 1979), 64-72.

Table 1. Statistical parameters of the design variables in containment example

Variable	Mean	c.o.v.	Distribution
D	1200 in.	0.0033	Normal
A_1	36 in^2	0.014	Normal
F_y	50,000 psi	0.10	Lognormal
X_0	1.00	0.12	Lognormal
t	1.00 in.	0.01	Normal
	1.25 in.	0.0096	
	1.50 in.	0.0105	
s_1	120 in.	0.00167	Normal
	180 in.	0.00167	
	240 in.	0.00167	

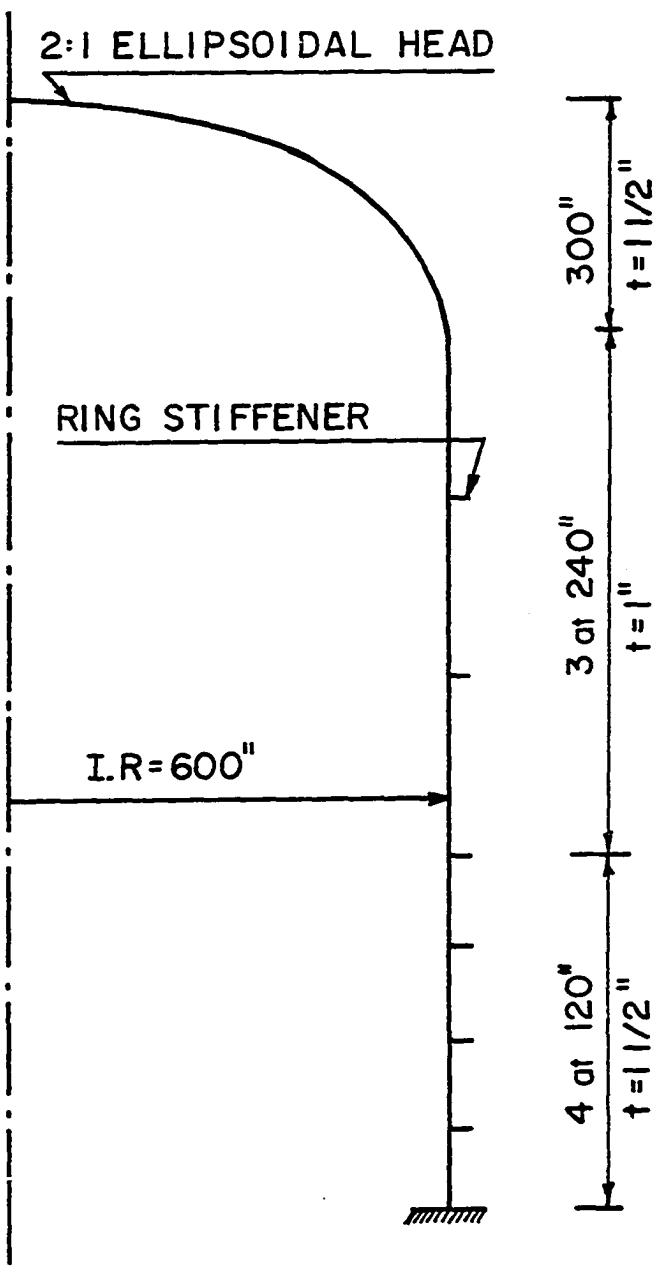

Figure 1. Containment vessel geometry

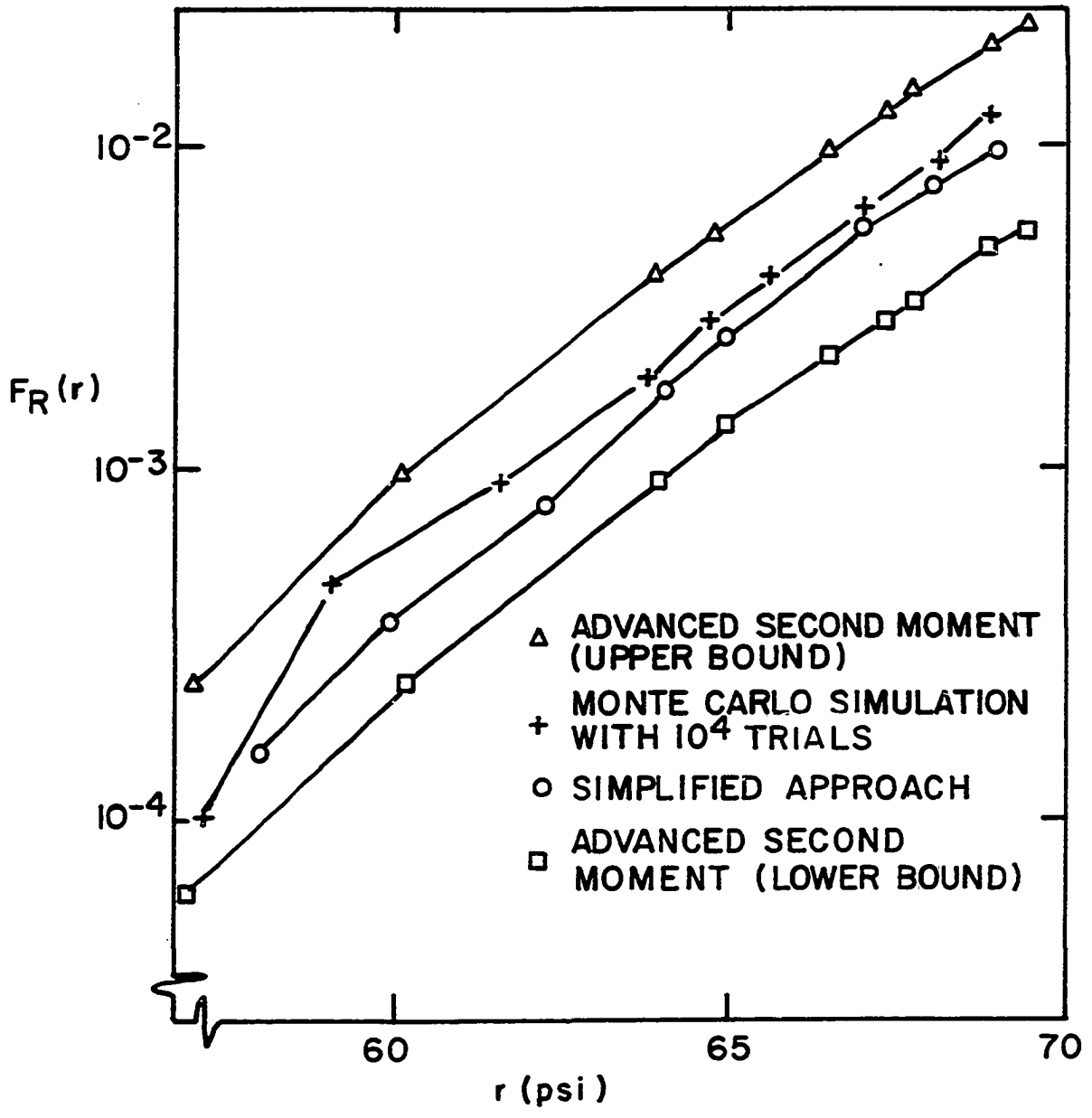

Figure 2. Cumulative distribution of the containment resistance

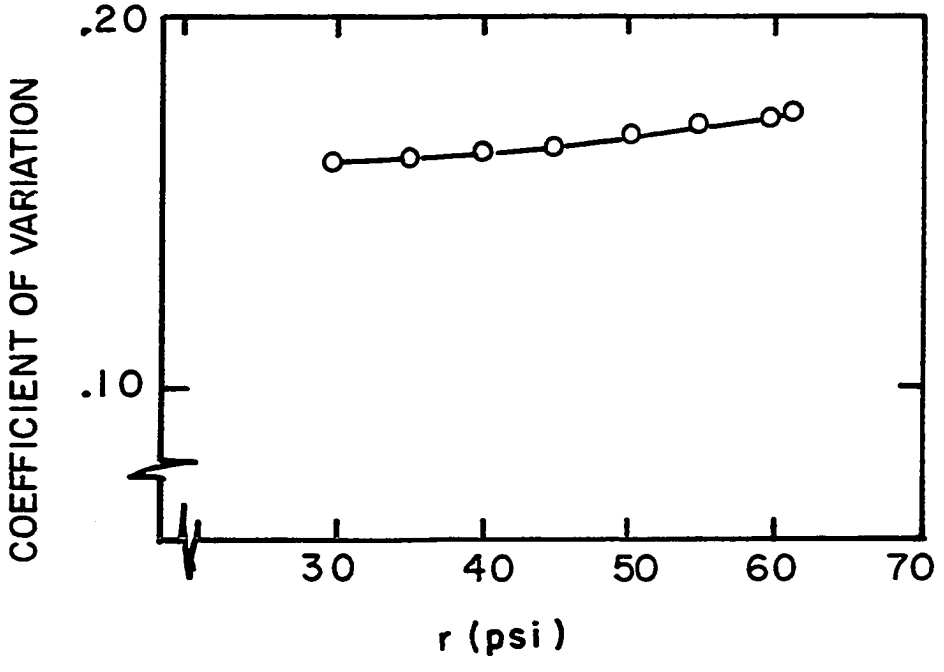

Figure 3. Coefficient of variation for the containment resistance

SUMMARY, CONCLUSIONS AND RECOMMENDATIONS

Summary

In spite of the extreme precautions that are considered in the design and construction of nuclear power plant containment vessels, leakage of radioactivity does have a non-zero probability of occurrence. To establish this probability, the structural design problem must be solved in light of a best estimate and uncertainty assessment of the containment resistance. In many cases, nonlinear finite element analysis has been used to analyze this type of structure. This is excessively expensive, particularly when all possible failure modes are required to perform the uncertainty analysis. An alternative approach to define the statistical characteristics of the containment vessel resistance is presented herein.

Simplified methods based upon limit analysis theory that account for the effect of large deformations are presented. Methods for the prediction of the resistance of stiffened axisymmetric containment vessels (cylinders, cones, hemispherical heads, ellipsoidal heads, torispherical heads) under uniform internal static pressure are developed. Finite element solutions were used to guide the formulation and to calibrate these methods. Twelve stiffened cylindrical shells were analyzed and the results were compared to the simplified methods results. Additionally, the nonaxisymmetric behavior that may be introduced due to the presence of the longitudinal stiffeners was investi-

gated. A solution of a stiffened panel was performed using three-dimensional and axisymmetric finite element models, respectively. Furthermore, a typical containment vessel was analyzed using the finite element and the proposed approaches.

Simplified dynamic analyses of locally loaded cylindrical shells, spherical shells and circular plates are given. The dynamic solutions are obtained by idealizing the system as an elastic-plastic single degree of freedom. Large deformation effects are included in the model. Several numerical examples are presented to demonstrate the use of the proposed simplified dynamic analysis methods. Again, finite element solutions were used to guide and calibrate the simplified solutions. An extensive study was conducted to investigate the effect of the time integration step size on the finite element results. The finite element geometric model and the impulse shape effects on the nonlinear transient dynamic analysis results were also investigated.

A study of various reliability analysis methods is conducted. Three different reliability assessments - Monte Carlo simulation, advanced first order second moment and simplified approach - are proposed. The Monte Carlo simulation technique was used to confirm the results of the other two approaches. A study indicated the insignificant effect of the randomness of particular variables, e.g., thickness and radius, on the reliability analysis. This finding was used to develop the simplified reliability approach proposed. The statistical characterization of a typical containment resistance is performed using these three reliability assessment techniques.

Conclusions

Static analysis of stringer stiffened axisymmetric cylindrical or conical shells under uniform internal pressure can be accomplished using an axisymmetric finite element idealization for the proportions studied. The longitudinal stiffener does not have a significant effect on the stiffened shell resistance when failure is due to shell and ring stiffener yielding (general mode). Plastic hinges form only at the rings while there is no moment midway between the rings when an inter-ring failure takes place. The simplified methods give good results when compared to the finite element results. Additionally, these methods are quite useful when performing the reliability assessment since they can predict each possible failure mode.

Nonlinear finite element dynamic results for impulsively loaded shells are sensitive to the time integration step size. To obtain an accurate solution with ANSYS, the problem should be solved with two different time step sizes, and the results should be linearly extrapolated to zero time step size. Deformations induced in an impulsively loaded shell are local, particularly as the structure reaches the nonlinear stage. A uniformly distributed pure impulse adequately approximates the pressure-time loading. The simplified dynamic analysis methods are sufficiently accurate to predict the strain ductility of cylindrical shells, spherical shells and circular plates. The strain ductility of these structures is practically independent of the radius of curvature.

The various reliability analysis methods presented, i.e., Monte Carlo simulation technique, advanced second moment method and the simplified reliability approach, can be used to define the statistical character of the containment vessel resistance. These methods require explicit formulations for each of the structural resistance modes, as provided by the simplified static and dynamic analysis methods. The simplified assessment approach is the most practical method to define the statistical parameters of the containment resistance.

Recommendations

Future work should be devoted to obtaining experimental results for stiffened and smooth shell structures with static and dynamic internal pressure. This would help to calibrate the simplified and finite element methods. A complete statistical characterization of the modeling error is required for the reliability analysis. Further studies of the behavior of impulsively loaded shells are needed. Such studies should investigate the wave propagation and convergence problem (time step size selection). Simplified dynamic analysis of stiffened shells would be useful for the reliability assessment since many of the containment vessels are provided with longitudinal and circumferential stiffeners. A reliability method which could be coupled with finite element analyses for these complex structures would yield more accurate results of the system resistance.

ACKNOWLEDGEMENT

The author wishes to express his sincere appreciation and thanks to his major professor, Dr. L. F. Greimann, for his help, guidance and suggestions during the research and writing of this dissertation. His aid, encouragement and understanding throughout the duration of the investigation is greatly appreciated. Thanks are also extended to Professor F. W. Klaiber, Professor F. M. Graham, Professor W. F. Riley and Dr. A. M. Wolde-Tinsae for serving on this writer's graduate committee. Finally, the author acknowledges the assistance of Dan Ketelaar, with ANSYS.

I also wish to thank my wife, Souzan, and my son, Peter, for their support during the ups and downs of my research and throughout the course of study.